國 立 交 通 大 學

應用化學系博士班

博士論文

奈米銀線之製備、性質與感測應用

Silver Nanowires: Preparation, Properties, and Sensing Applications

研 究 生：蕭暐翰

指導教授：裘性天 博士

李紫原 博士

中華民國一百年十一月

Contents

List of Tables

Chapter 1

Chapter 3

Chapter 4

Appendix

List of Figures

Chapter 1

Chapter 2

Chapter 4

Silver Nanowires: Preparation Properties and Sensing Applications

Student: Wei-Han Hsiao Advisor: Dr. Hsin-Tien Chiu

Dr. Chi-Young Lee

Ph. D program

Department of Applied Chemistry

National Chiao Tung University

Abstract

In this thesis, we demonstrate a simple low-cost galvanic reduction with surfactant-assisted method to grow urchin-like Ag nanowires (NWs) on electrodes.

First, urchin-like Ag NWs on screen-printed carbon (SPC) electrodes were prepared via glavanic reductions of $AgNO_{3(aq)}$ solutions in the presence of cetyltrimethylammonium chloride (CTAC) by Cu foil. The diameters of the nanowires are about 80-120 nm, and their lengths are up to 10 μm. The Ag NW is single crystalline and tends to grow along the [110] direction. Moreover, we can use electrochemical deposition to synthesize Ag NW on Au or Pt seeding layers on Indium Tin Oxide (ITO) substrates with similar reaction condition.

The second subject is surface plamon resonance (SPR) property of urchin-like Ag NWs. The absorption peak at ca. 380 nm was attributed to the plasmon response from the transverse mode of the NWs while the broad band extended from 500 nm was assigned to the longitudinal modes of the NWs with different aspect ratios. Furthermore, we used Rhodamine 6G as the probe molecule, and the the excitation wavelength of 532 nm was applied for the surface enhanced Raman scattering (SERS)

experiments. The detection limit of Rhodamine 6G on the urchin-like Ag NWs can be as low as 10^{-16} M while the analytical enhancement factor is about 10^{13}. Raman mapping images confirm that a single R6G molecule on the substrate can be detected.

The final subject is hydrogen peroxide sensing application. Cyclic voltammetric experiments using the Ag NWs as the working electrode showed electrocatalytic H_2O_2 reduction. For H_2O_2 sensing, the electrode exhibited a high sensitivity of 4705 μA mM^{-1} mg^{-1} cm^{-2} from 50 μM to 10.35 mM and a measurable detection limit of 10 μM in amperometric detection. This is the first report on Ag NWs for non-enzymatic H_2O_2 sensing.

奈米銀線之製備、性質與感測應用

研究生：蕭暐翰　　指導教授：裘性天 博士

李紫原 博士

國立交通大學應用化學系博士班

摘要

在本論文中，我們以賈凡尼還原法配合界面活性劑(烷基三甲基氯化銨)輔助成長法，成功地將海膽狀奈米銀線成長於電極上。

首先，我們利用銅與硝酸銀的賈凡尼自發性氧化還原反應，在含有十六烷基三甲基氯化銨與硝酸的水溶液中成長海膽狀奈米銀線於市售網版印刷碳電極上，其直徑約為 80-120 nm，藉由不同的反應時間，長度可達 10 μm 左右。經由結構分析顯示奈米銀線為單晶且成長方向為[110]。除此之外，我們也利用類似的反應溶液，在鍍有金或鉑的氧化銦錫(ITO)導電玻璃上，以電化學沉積法也能得到奈米銀線。

第二部分我們利用海膽狀奈米銀線，觀察其表面電漿共振特性。研究發現，奈米銀線在紫外光區有表面電漿共振吸收特性，其主要吸收位置在 380 nm 與 500 nm 附近。我們更進一步的深入討論其在表面增強拉曼散射之應用，結果顯示當我們以 532 nm 的雷射光作為激發光源，並以染料分子(Rhodamine 6G)作為偵測分子，可以得到最佳的偵測極限為 10^{-16} M，其分析增強因子(Analytical Enhancement Factor)為 10^{13}。利用表面增強拉曼光譜影像分析(SERS mapping images)，證明其有單分子偵測(single molecule detection)能力。

最後我們利用海膽狀奈米銀線作為電極，進行過氧化氫電化學感測實驗。循環伏安法實驗展示海膽狀奈米銀線具有增強電催化過氧化氫還原的能力，在過氧

化氫安培法感測中，此電極展現高靈敏度(4705 μA mM^{-1} mg^{-1} cm^{-2})，其偵測範圍為 0.05 mM-10.35 mM，偵測極限可達 10 μM。這也是第一個利用奈米銀線作為非酵素型過氧化氫感測應用(non-enzymatic H_2O_2 sensing application)。

Acknowledgement

時光匆匆，沒想到我也有這一天。在交大念了十一年多的書，總算要離開，感覺很不真實，也非常的開心。打從大三專題生起，就接受了裘性天老師的指導，雖然我的個性並不細心，但隨著專題生，碩士班，到現在博士班可以畢業，全是在裘老師叮嚀下，讓我在科學研究領域上，能有些微的成果與貢獻，甚至在人生的道路上，也得到更多的經驗與指導。而在研究所期間，李紫原老師多元的想法與建議，也讓我在思考研究上有更多的心得與收穫，更感謝老師們能參與我的終生大事，讓我感到異常光榮。

感謝各位口試委員給予我論文的指導，黃暄益老師與李積琛老師在金屬材料成長與光譜上的建議，以及廖奕翰老師在拉曼光譜數據上的指導，讓學生的論文更加詳細清楚，也解決了許多內容上的缺失。

在研究的生活中，實驗室的夥伴是不可或缺的，上從大我七屆的學長，下至小我七屆學弟妹，擁有你們這群生活上的夥伴，讓研究生的生活除了研究，也增添了許多快樂的回憶，也因為這些 chiulab 的夥伴，使得大家在實驗不順遂時，除了老師之外，你們大家提供了各式各樣的幫助，包括研究上與精神上，這都是在我博士生涯中不可或缺的。

最後要感謝我的家人，爸媽一直都很擔心我是否能畢業，卻也不增添我的壓力，岳父岳母更力挺我能順利的渡過這個人生的轉捩點。我的老婆，真的是讓妳辛苦了，有妳的支持與諒解，我才能在最後這一年無後顧之憂的全力為我的論文奮戰，也感謝有妳，我才能順利擁有一個獨一無二的兒子，也因為有妳們這些家人，我才真正體會到什麼是娶某前生子後的好運氣，這一切的一切，都要感謝你們！

最後的最後，我要跟大家說句經典名言：我要走了！

Chapter 1

Introduction

1.1 Introduction

As we know, silver is widely used in our daily life such as jewelry, currency, mirrors and optics.[1] In medical usage, silver compounds have been used to prevent infection in World War I before the advent of antibiotics.[2] There are a lot of silver applications such as dentistry, photonics, photography, catalysis, electronics nowadays.[3-5] In addition, bulk silver exhibits the highest electrical and thermal conductivities among all metals. Therefore, the exploration of silver applications is an important topic in future science.

One-dimensional (1D) nanostructures (nanowire (NW), nanorod (NR), and nanotube (NT)) have been the focus of many recent studies due to their potential application in both interconnects and functional units of fabricating electronic, photonic, and sensing devices, which also provide an ideal model system to experimentally investigate physical phenomena, such as quantized conductance and size effects.[6-19] Consequently, the synthesis and characterization of NWs have recently attracted attention from a great deal of researchers.[20-23] Based on the unusual chemical and physical properties of 1D nanomaterials associated with the size and shape,[24] lots of researchers have demonstrated that single one or arrays of 1D nanomaterials used as a building block in electronic, photonic, and sensing devices, which could attain miniaturization and enhance the performance. Among them, noble metal nanomaterials displays surface plasmon resonance (SPR),[25] surface-enhanced Raman scattering (SERS),[26] and electrochemical catalytic properties, which become a popular

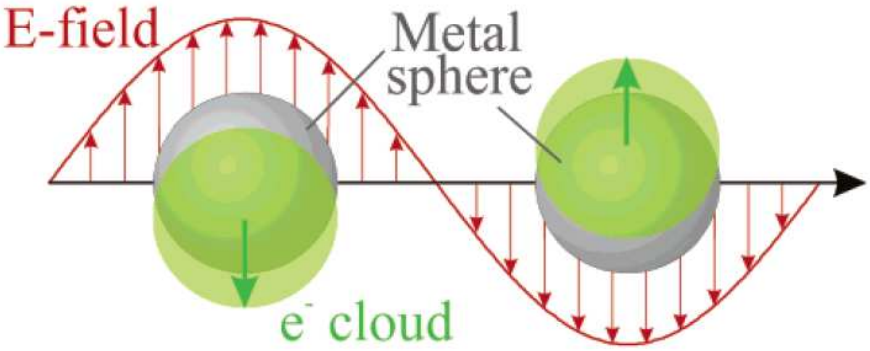

Figure 1.1 Schematic of plasmon oscillation for a sphere, showing the displacement of the conduction electron charge cloud relative to the nuclei.[28]

research subject. Until now, there have been few reports of 1D noble metal nanomaterials which are direct grown on hard template and their potential applications.

In this dissertation, 1D noble metal nanomaterials (urchin-like Ag NWs) were fabricated by surfactant assisted electrochemical methods. The intrinsic properties of urchin-like Ag NWs such as SERS performance and electrochemical catalysis would be investigated.

1.2 Properties and Applications of Silver Nanomaterials

1.2.1 Surface Plasmon Resonance (SPR) Absorption

It is interesting to see metal nanoparticles (NPs) with different colors. For examples, Au colloidal NPs are brilliant red and Ag NPs are typically yellow. In the middle 1800s, Michael Faraday synthesized colloidal solutions of gold exhibiting colors range from rube red to amethyst.[27] The various colors resulted from the surface plasmon band (SPB), which is a phenomenon observed in transmission, due to the presence of NPs, in solution or in the solid phase. When a small spherical metallic NP is irradiated by light, the oscillating electric field causes the conduction electrons to oscillate coherently (show in Figure 1.1).[28] When the electron cloud is displaced

relative to the nuclei, a restoring force arises from Coulomb attraction between electrons and nuclei that results in oscillation of the electron cloud relative to the nuclear framework.

In 1908, Mie presented a solution to Maxwell's equations[29-31] that describes the extinction spectra (extinction = scattering + absorption) of spherical particles of arbitrary size. Until now, several numerical techniques based on finite elements have been demonstrated the limitation in calculations of particles with arbitrary shape and muitcomposition.[32,] Among them, the discrete dipole approximation (DDA) has been proven to be an effective technique for estimating the optical properties of metal NPs.[33] The extinction spectra of metal NPs under various conditions were mostly simulated by the DDA calculation and compared with the experimental results.[34] The influence of particle shapes on SPR wavelengths was also investigated.

The particle size, shape, and intrinsic dielectric constant are an important factor to the SPR wavelength. A lot of researches concerning the size effect of spherical NPs have been reported.[35] Besides, the geometry of metal particles also have strong influences on the SPR peaks such as nanoprisms and nanocubes. The phenomenon is usually occurred in Ag nanomaterials with different shapes. For example, Schatz and co-workers have illustrated that the increase of the side length of Ag nanoprisms could lead their SPR peak to red shift by several hundred nanometers.[36] In the case of Ag NRs or NWs, there are two SPR peaks which would change with the aspect ratio of the Ag 1D nanomaterials.[25] This is due to the absorption of visible light both along the length of the nanorod (the longitudinal plasmon band) and along the width of the nanorod (the transverse plasmon band). The larger the aspect ratio, the more red-shifted the longitudinal plasmon band, as theory predicts[37] and experiment confirms.[38-42]

This controllable optical property in terms of wavelength is quite exciting and

Table 1.1 Comparison of the Suitability of Different Metals for Plasmonic Applications.[50]

Metal	plasmonic ability	chemical	nanostructure formation	cost (per ounce)[a]
aluminum (Al)	good in UV region	stable after surface passivation	very few nanostructures; used in lithographic patterning	$0.066
copper (Cu)	interband transitions below 600 nm	easy oxidation	very few nanostructures	$0.25
gold (Au)	interband transitions below 500 nm; high quality factor	very stable; biocompatible	many nanostructures	$1859.6
palladium (Pd)	low quality factor; not suitable for plasmonics	Stable	many nanostructures	$742
platinum (Pt)	low quality factor; not suitable for plasmonics	Stable	many nanostructures	$1837
silver (Ag)	highest in quality factor (300 nm~1200 nm)	oxidation; biocompatibility issues	many nanostructures	$41.48

a: metal cost (2011/9/11) can be found at the Web site: http://www.kitco.cn/hk/metal-market/precious-metals/precious-metals-market.htm

interesting, and it enables the particles to be applied in biological sensing and drug delivery.[43,44] As a result, silver is probably the most important material in plasmonics. It offers many advantages over Au, Cu, and Al which are other metals known to support surface plasmons (SPs) in the visible (vis) and near-infrared regions (NIR).[45,46] In terms of plasmonics, it is important to choose a metal that can support a strong SP at the desired resonance wavelength.[47,48] The SP strength is directly proportional to the quality factor (Q).[46] Ag has the largest quality factor across most of the spectrum from 300 to 1200 nm. In contrast, Al is only suitable for applications in the ultraviolet (UV) region. For Au and Cu, their SPR excitation wavelengths are longer than 500 and 600 nm, respectively.[49] Furthermore, the difficulty of fabricating nanostructures, and their cost, will also determine the usefulness of a metal for SPR applications, especially for large-scale applications. As shown in Table 1.1, silver is relatively cheap among the metals that support plasmons and easy to fabricate.[50] To

sum up, Ag compared with the other metals is unique for its excellent qualities in terms of SPR ability, available nanostructures, and material cost.

1.2.2 Surface-Enhanced Raman Scattering (SERS)

In 1928, Indian scientist Sir C. V. Raman observed the Raman effect by means of sunlight and won the Nobel Prize in Physics in 1930. Raman spectroscopy displays the change in wavelength that is attributed to the excitation (or relaxation) of vibrational modes of a molecule when a photon undergoes Raman scattering. Since vibrational information is specific to the chemical bonds and symmetry of molecules. Therefore, each molecule can be identified and shows a unique fingerprint in a Raman spectrum. In accordance with the Raman selection rule, the molecular polarizabilty changes as the molecular vibrations displace the constituent atoms from their equilibrium positions. The amount of the polarizability change will determine the Raman scattering intensity. Hence, aromatic molecules usually exhibit more intense Raman scattering than aliphatic molecules.

In general, Raman spectroscopy has lots of advantages for microscopic analysis. For examples, specimens do not need to be fixed or sectioned; Raman spectra can be collected from a very small volume (< 1 μm in diameter); water does not generally interfere with Raman spectral analysis. However, there are some limitations for the applicability of Raman scattering such as the intrinsic small intensity of the Raman signal, the sensitivity limit of available detectors, and the intensity of the excitation source.

In 1974, SERS from pyridine adsorbed on electrochemically roughened silver was produced by Martin Fleischman and coworkers.[51] After that, Jeanmaire and Van Duyne demonstrated that the magnitude of the Raman scattering signal can be greatly enhanced when the scattering is placed on or near a roughened noble metal substrate.[26] This is called electromagnetic effect, which is one of the SERS

mechanisms. Strong electromagnetic fields are generated when the localized surface plasmon resonance (LSPR) of nanoscale roughness features on silver or gold substrates is excited by visible light. When the Raman scatterer is subjected to these intensified electromagnetic fields, the magnitude of induced dipole increases, and accordingly, the intensity of the inelastic scattering increases. This is the main factor in SERS. The other factor is called chemical effect,[52] which is contributing enhancement only on the order of an order or two of magnitude.[53] The chemical enhancement involves changes to the adsorbate electronic states due to chemisorption of the analyte which results in charge transfer between metal and adsorbate. Until now, the exact mechanism of the enhancement effect of SERS is still a matter of debate in the literature. These two factors are generally approved.

In order to know the performance of the SERS, definitions of SERS enhanced factor (EF) have been investigated. The most widely used definition for the average SERS EF equation is shown below:[54]

$$EF=(I_{SERS}/N_{Surf})/(I_{RS}/N_{Vol}) \quad (1.1)$$

where N_{Vol} is the average number of molecules in the scattering volume (V) for the Raman (non SERS) measurement, and N_{Surf} is the average number of adsorbed molecules in the scattering volume for the SERS experiments.

The rigorous definition:

$$N_{surf}=\mu_M\mu_S A_M A_{eff} \quad (1.2)$$

$$N_{vol}=C_{RS}V=C_{RS}H_{eff}A_{eff} \quad (1.3)$$

where μ_M is the surface density of the individual nanostructures with respect to the main plane forming the substrate, μ_S is the surface density of molecules on the metal, A_M is the metallic surface area in each nanostructure, C_{RS} is the concentration used for the non-SERS spectra, H_{eff} is the effective height of the scattering volume, and A_{eff} is the effective surface area of the scattering volume (the equivalent of a scattering

volume but for 2D).

As a result of the complicated definition, all the factors are not easy to ensured or estimated in every experimental condition.

The definitions described above have attempted to emphasize the intrinsic characteristics of the substrate and are not always straightforward to relate to experimental results. For many applications, however, one is mostly concerned with the simple question of how much more signal can be expected from SERS as compared to normal Raman under given experimental conditions. To address this question, another definition of SERS EF which is fairly intuitive and particularly relevant for analytical chemistry applications is introduced. It is called the analytical enhancement factor (AEF) which is presented by the equation:[54]

$$AEF=(I_{SERS}/C_{SERS})/(I_{RS}/C_{RS}) \quad (1.4)$$

Here, I_{RS} represents the Raman intensity of an analyte with a concentration C_{RS} on a non-SERS substrate. I_{SERS} is obtained from a SERS-active substrate with an analyte concentration C_{SERS}. In the experiments, all the other parameters, including laser wavelength, laser power, microscope magnification, and spectrometer are identical. The AEF in fact ignores the fact that SERS is a type of surface spectroscopy, which means that only the adsorbed molecules contribute to the signal, and that the effect is distance dependent.

Nowadays, SERS can be exploited for sensitive and selective molecular identification. In 1997, Shuming Nie has successfully proved that single rhodamine 6G (R6G) molecule could be probed with Ag NPs by SERS.[55] In recent years, other single molecule detections have been reported, too.[56-65] Therefore, SERS has been used extensively as a signal information in biological and chemical sensing such as protein,[66-68] DNA[69,70], and environmental pollutants.[71-74] A miniaturized, inexpensive, and portable SERS instrument makes the technique practical for trace analysis in

clinics, the field, and urban settings.[75]

1.2.3 Catalytic Properties

Silver is a common heterogeneous catalysis in the chemical industry. It can synthesize various chemicals and reduce production cost. For example, the selective oxidation of ethylene to ethylene epoxide (also known as ethylene oxide) is an important industrial catalytic reaction. Silver is considered almost the unique effective catalyst for ethylene epoxidation[76] and α-Al_2O_3 is the preferred support. Moreover, Styrene ($C_6H_5CH=CH_2$) and epoxides are industrially important bulk chemicals, which are largely used for synthesis of several perfumes, epoxy resins, plasticizers and drugs. Epoxidation of styrene to styrene oxide (SO) by molecular oxygen was also studied using the silver catalysts.[77]

Reduction of 4-aminophenol (4-AP) is also an important subject and the conventional methods for hydrogenation of 4-NP involve iron/acid as a reducing agent.[78] The reason is that manufacturing of many analgesic and antipyretic drugs, such as paracetamol, phenacetin, and so on, needs 4-AP as a potent intermediate. It is also used enormously as a photographic developer, corrosion inhibitor, anticorrosion-lubricant, and hair-dyeing agent.[79,80] As we know, reduction of aromatic nitro compounds is inert to sodium borohydride ($NaBH_4$) reaction if it is used alone. Catalytic reduction of aromatic nitro compounds by coinage metal nanoparticles has been reported.[81] Here, Ag nanomaterials have also shown their worth for catalytic reduction of 4-AP by using $NaBH_4$ as an alternative effective and eco-friendly method.[82,83]

1.2.4 Electrochemical Property and Sensing

Electrochemical reactions taking place at the interface between flat electrodes and electrolyte solutions are often impeded by diffusion process. In order to overcome this problem, fabrication of nanostructured electrodes with the high roughness (ratio of

real surface area to geometric area) are developed. These electrodes display high electrochemical active surface areas and accelerate the electrochemical reactions. Therefore, there are many NP-modified electrodes fabricated such as silver, gold, and platinum NP electrodes which are used as a excellent electron transfer mediator.[84-86]

The size dependent electrocatalytic behaviors of nanomaterials of silver, platinum and gold has been demonstrated previously.[87-91] Moreover, electrocatalytic behaviors on various morphology of nanomaterial electrodes have been investigated in recent years.[92-101] In general it is accepted that catalytic activity is related to the surface energy of exposed crystal faces. The structure of low-index planes are regarded as surface defects play a significant role in electrocatalysis.[102-104]

Silver is a highly active electrocatalyst in alkaline solutions for the oxidation of small organic molecules, due to the formation of reactive adsorbed OH species that influence the kinetics of the reaction.[93,102,105-109] Also, it has been demonstrated that nanosized Ag can act as an effective sensing material for the detection of pesticides[110] and toxic substances such as lead[111] as well as important species such as hydrogen peroxide,[108,112] nitrates,[113-115] and hydrazine.[116]

1.3 Various Synthetic Strategies of 1D Metal Nanomaterials

1.3.1 Direct Hard Template Method

In general, channels in porous membranes provide a typical template for use in the synthesis of 1D nanostructure (Fig 1.2).[24] This method was demonstrated by Martin and several others.[117-119] Until now, anodic aluminum oxide (AAO) is the most widely used hard template.[120] Figure 1.2 shows that NWs and NTs can be formed by full and part filled channels with desire materials, respectively.[121-123] For example, Wu et al. and Choi et al. have employed AAO-assisted electrochemical deposition to fabricate Ag NWs with adjustable diameter and high aspect ratio.[124,125] Other hard templates such as step-edge surface,[126] DNA molecules[127,128] have also reported.

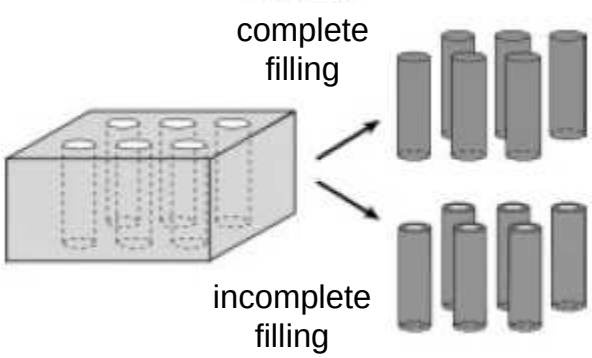

Figure 1.2 Scheme of NWs and NTs formation by filling and partial filling the pores within a porous membrane with the desired material or precursor to this material.[24]

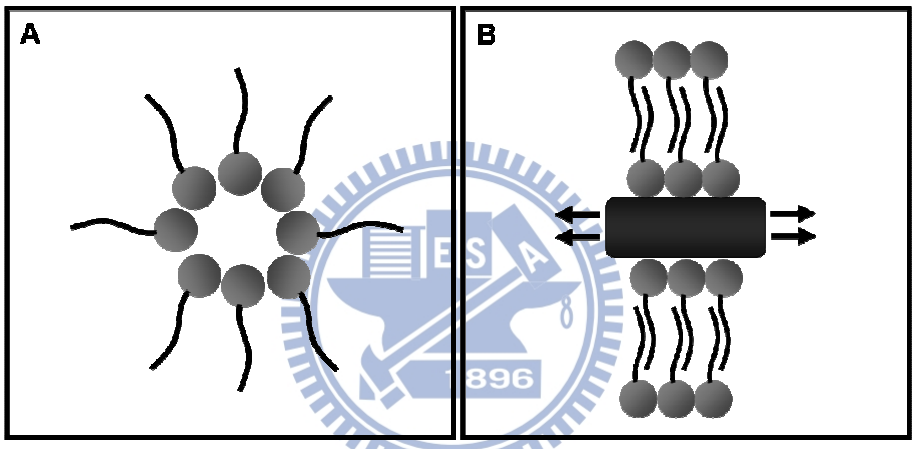

Figure 1.3 (A) self-assembled reverse micelle and (B) capping reagent mechanism of surfactants.[129]

1.3.2 Micelle and Reversed Micelle Methods

This method is also called soft template method which is the early procedure for fabricating NPs. Surfactants have both hydrophilic and hydrophobic tails and self-assemble into reversed micelles with various shapes in aqueous solution, as show in Figure 1.3A.[129] Nanocrystals are formed by reducing metal ions in this microreactor and stably dispersive in solution.[130,131] Hong et al. used the pores of self-assembled calix[4]hydroquinone nanotubes as a soft template to synthesize ultrathin single crystalline Ag NWs arrays by electro/photochemical redox reaction in

an ambient aqueous phase.[132]

1.3.3 Seed-Mediated Growth

Murphy and coworkers have developed seed-mediated growth to fabricate and contol 1D metal nanomaterials.[25] The procedure begins with the synthesis of metallic nanospheres by chemical reduction of a metal salt with a strong reducing agent such as $NaBH_4$. Citrate is present as a capping agent to prevent particle growth. The gold or silver spheres thus generated are 3±5 nm in diameter and serve as seeds on which to grow more anisotropic nanostructures. When adding seeds into the reaction solution contained metal salts, weak reducing agent, and surfactants, the reaction would be activated and metal atoms could deposit selectively on the seeds to form anisotropic growth. NRs and NWs with an uniform diameter and controllable aspect ratio were fabricated in the presence of 4 nm Ag seeds, $AgNO_3$/ ascorbic acid growth solution and cetyltrimethylammonium bromide (CTAB).[41] For Au NRs, the synthesis is similar, too.[42] Figure 1.3B displays that bilayer structures of surfactants (CTAB) self-assemble adsorbed selectively on specific crystal facets and confine their growth.[129] The relative growth rate between capped and uncapped sites results in the formation of NRs or NWs. CTAB, called capping reagent, play an important role for controlling anisotropic crystal growth.

1.3.4 Polyol Process

Xia and coworkers recently demonstrated a poloyol method that generated Ag NWs by reducing $AgNO_3$ with ethylene glycol in the presence of poly(vinyl pyrrolidone) (PVP).[133,134] Ethylene glyol served as both solvent and reducing agent. The key to formation of wire-like nanostructures is the introduction of exotic seeds (Pt NPs) to the reaction mixture and the using of PVP as a polymeric capping reagent which adsorbed on Ag nanocrystal surfaces by O atoms confirmed by X-ray photoelectron spectra (XPS).[135]

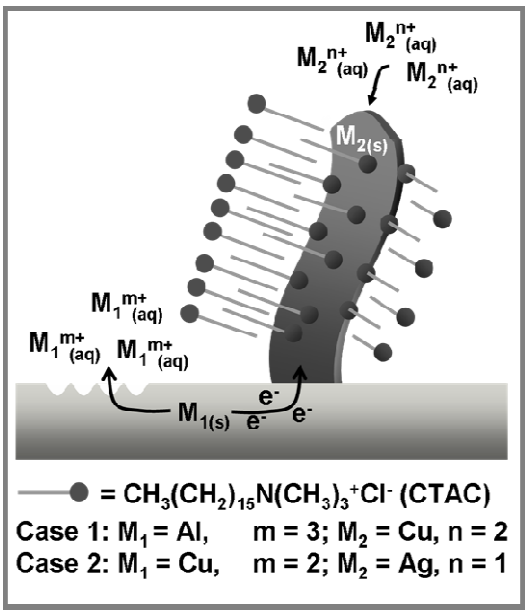

Figure 1.4 Scheme of growth mechanism of Cu Nanobelt and Ag Belt-like materials.[136]

1.3.5 Galvanic Displacement Reduction

Most of methods described above are homogeneous solution reaction. In 2007, we evolved heterogeneous galvanic displacement reduction to fabricate Cu and Ag nanobelts (NBs).[136] Sacrificial metals oxidized itself and reduced the other metal ions at the interface of metal and solution as shown in Figure 1.4. We used cetyltrimethyl-ammonium chloride (CTAC) as a capping reagent to successfully grow and immobilize the diverse nanostructures on electrodes at the same time. Moreover, we also fabricate Cu NBs[137] and Au NWs[138,139] on electrodes in similar reaction condition by electrochemical deposition.

1.3.6 Vapor-Solid Reaction Growth (VSRG)

Our group develop a route of vapor solid reaction growth to synthesize cable-like Cu and Ag NWs.[140,141] CuCl encapsulated in poly(dimethylsiloxane) (PDMS) and tetrakis(trimethylsilyl) silane (TTMS, $Si(SiMe_3)_4$) as a reducing agent were sealed in a Pyrex tube under low pressure and reacted in the furnace under 473 K for 6 h. After

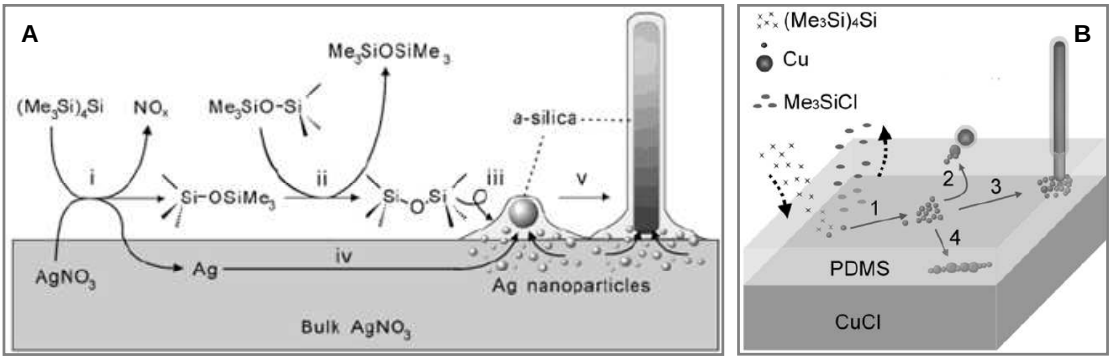

Figure 1.5 Scheme of cable-like NWs growth mechanism (A) Ag/SiO_2 NWs (B) Cu/PDMS NWs.[140,141]

the reaction, cable-like Cu/PDMS NWs were produced. On the other hand, $AgNO_3$ and $(Me_3Si)_4Si$ were reacted in a sealed tube under low pressure at 400 K in 10 min and held at the temperature for 2 h and cable-like Ag/SiO_2 NWs were generated. Figure 1.5 display the mechanisms of growth cable-like Cu and Ag NWs.[140,141]

1.3.7 Arc Discharge Method

An electric arc is an electrical breakdown of a gas which produces an ongoing plasma discharge, resulting from a current flowing through normally nonconductive media such as air. Arc discharge process is the first and now widespread method of carbon NTs production. Wang et al. reported that high density and high purify Ag-core/C-shell nanocables could be synthesized via a hydrogen arc discharged method.[142] The cathode was a solid randomly oriented graphite (ROG) rod, and the anode is a cup-like ROG rod filled with carbon black and Ag powder. The diameter of the Ag-core is dependent on the percentage of Ag present in the anode.

1.3.8 Solid-Liquid Phase Arc Discharge (SLPAD) Method

Zhou and coworkers report a novel method for preparation of silver nanowires via a so-called solid liquid phase arc discharge method (SLPAD).[143] High-purity silver filaments were used as two electrodes and $NaNO_3$ was used as electrolyte. It formed the instantaneous circulation between the two electrodes and arc discharge sparks

while a certain voltage was used. It is well-known that the arc discharge released great exothermic heat, leading to the occurrence of the continuous dissolution of silver electrodes in a form of silver clusters. These clusters entered into $NaNO_3$ solution in a possible shape of the tadpole-like or column-like morphology and the cooling water will restrain the contraction of these shaped clusters and prevented them from becoming spherically shaped. These factors may be favorable for the formation of the Ag NWs.

1.4 Aim of This Thesis

In recent years, there are great deals of reports about synthesizing Ag nanomaterials due to their interesting morphology related chemical and physical properties. Among them, many researchers are interested in sensing applications of Ag nanomaterials such as SERS and electrocatalysis. Until now, most of Ag nanomaterials synthetic methods require multiple steps, strict conditions, and cost much. Especially, there are few reports regarding direct growth of 1D Ag nanomaterials on electrodes for sensing applications in the past years.

In this thesis, we demonstrate a simple low-cost surfactant-assisted galvanic reduction process to direct grow urchin-like Ag NWs on carbon screen printed electrodes. According to the intrinsic properties of Ag, SERS and electrocatalysis sensing applications of urchin-like Ag NWs are investigated. The detail studies would be presented in the following chapters.

1.5 References

1. Wilson, Ray N. *Reflecting Telescope Optics: Basic design theory and its historical development.* Springer. **2004** p. 422.
2. Medical uses of silver can be found at the Web site: http://en.wikipedia.org/wiki/Medical_uses_of_silver#cite_note-31
3. Jin, R.; Cao, Y.; Mirkin, C. A.; Kelly, K. L.; Schatz, G. C.; Zheng, J. G. *Science* **2001,** *294*, 1901.
4. Hoelderich, W. F. *Catal. Today* **2000,** *62*, 115.
5. Gould, I. R.; Lenhard, J. R.; Muenter, A. A.; Godleski, S. A.; Farid, S. *J. Am. Chem. Soc.* **2000,** *122*, 11934.
6. Favier, F.; Walter, E. C.; Zach, M. P.; Benter, T.; Penner, R. M. *Science* **2001,** *293*, 2227.
7. Cui, Y.; Wei, Q.; Park, H.; Lieber, C. M. *Science* **2001,** *293*, 1289.
8. Gudiksen, M. S.; Lauhon, L. J.; Wang, J.; Smith, D. C.; Lieber, C. M. *Nature* **2002,** *415*, 617.
9. Hu, J.; Odom, T. W.; Lieber, C. M. *Acc. Chem. Res.* **1999,** *32*, 435.
10. Sun, L.; Searson, P. C.; Chien, C. L. *J. Chem. Phys.* **2001,** *79*, 4429.
11. Peng, X. *Adv. Mater.* **2003,** *15*, 459.
12. Iijima, S. *Nature* **1991,** *354*, 56.
13. Ebbesen, T. W.; Ajayan, P. M. *Nature* **1992,** *358*, 220.
14. Morales, A. M.; Lieber, C. M. *Science* **1998,** *279*, 208.
15. Han, W.; Fan, S.; Li, Q.; Hu, Y. *Science* **1997,** *277*, 1287.
16. Dai, H.; Wong, E. W.; Lu, Y. Z.; Fan, S.; Lieber, C. M. *Nature* **1995,** *375*, 769.
17. Saito, S. *Science* **1997,** *278*, 77.
18. Bockrath, M.; Cobden, D. H.; McEuen, P. L.; Chopra, N. G.; Zettl, A.; Thess, A.; Smalley, R. E. *Science* **1997,** *275*, 1922.

19. Suenaga, K.; Colliex, C.; Demoncy, N.; Loiseau, A.; Pascard, H.; Willaime, F., *Science* **1997,** *278*, 653.

20. Lu, Q.; Gao, F.; Komarneni, S. *Langmuir* **2005,** *21*, 6002.

21. Dai, Y.; Zhang, Y.; Bai, Y. Q.; Wang, Z. L. *Chem. Phys. Lett.* **2003,** *375*, 96.

22. Qian, W.; Wei, F.; Liu, T.; Wang, Z. W. *Solid State Commun.* **2003,** *126*, 365.

23. Gundiah, G.; Deepak, F. L.; Govindaraj, A.; Rao, C. N. R. *Chem. Phys. Lett.* **2003,** *381*, 579.

24. Xia, Y.; Yang, P.; Sun, Y.; Wu, Y.; Mayers, B.; Gates, B.; Yin, Y.; Kim, F.; Yan, H. *Adv. Mater.* **2003,** *15*, 353.

25. Murphy, C. J.; Jana, N. R. *Adv. Mater.* **2002,** *14*, 80.

26. Jeanmaire, D. L.; Van Duyne, R. P. *J. Electroanal. Chem.* **1977,** *84*, 1.

27. Faraday, M. *Philos. Trans.* **1857,** *147*, 145.

28. Kelly, K. L.; Coronado, E.; Zhao, L. L.; Schatz, G. C. *J. Phys. Chem. B* **2002,** *107*, 668.

29. Mie, G. *Ann. Phys.* **1908**, *25*, 377.

30. Kerker, M. *The Scattering of Light and Other Electromagnetic Radiation*; Academic: New York, **1969**.

31. Bohren, C. F.; Huffman, D. R. *Absorption and Scattering of Light by Small Particles*; Wiley Interscience: New York, **1983**.

32. Waterman, P. C. *Phys. Rev. D* **1971**, *3*, 825.

33. Yang, W. H.; Schatz, G. C.; Duyne, R. P. V. *J. Chem. Phys.* **1995**, *103*, 869.

34. Duval Malinsky, M.; Kelly, K. L.; Schatz, G. C.; Van Duyne, R. P. *J. Phys. Chem. B* **2001**, *105*, 2343.

35. Messinger, B. J.; von Raben, K. U.; Chang, R. K.; Barber, P. W. *Phys. Rev. B* **1981**, *24*, 649.

36. Jin, R.; Charles Cao, Y.; Hao, E.; Metraux, G. S.; Schatz, G. C.; Mirkin, C. A.

Nature **2003**, *425*, 487.

37. El-Sayed, M. A. *Acc. Chem. Res.* **2001**, *34*, 257.
38. Foss, C. A.; Hornyak, G. L.; Stockert, J. A.; Martin, C. R. *J. Phys. Chem.* **1994**, *98*, 2963.
39. Yu; Chang, S.-S.; Lee, C.-L.; Wang, C. R. C. *J. Phys. Chem. B* **1997**, *101*, 6661.
40. Link, S.; Mohamed, M. B.; El-Sayed, M. A. *J. Phys. Chem. B* **1999**, *103*, 3073.
41. Jana, N. R.; Gearheart, L.; Murphy, C. J. *Chem. Commun.* **2001**, 617.
42. Jana, N. R.; Gearheart, L.; Murphy, C. J. *J. Phys. Chem. B* **2001**, *105*, 4065.
43. West, J. L.; Halas, N. J. *Annu. Rev. Biomed. Eng.* **2003**, *5*, 285.
44. Moores, A.; Goettmann, F. *New J. Chem.* **2006**, *30*, 1121.
45. Wiley, B.; Sun, Y.; Xia, Y. *Acc. Chem. Res.* **2007**, *40*, 1067.
46. Ru, E. L.; Etchegoin, P. *Principles of Surface Enhanced Raman Spectroscopy*; Elsevier: Oxford, U.K., **2009**.
47. Lal, S.; Link, S.; Halas, N. J. *Nat. Photonics* **2007**, *1*, 641.
48. Link, S.; El-Sayed, M. A. *J. Phys. Chem. B* **1999**, *103*, 8410.
49. Wang, H.; Tam, F.; Grady, N. K.; Halas, N. J. *J. Phys. Chem. B* **2005**, *109*, 18218.
50. Rycenga, M.; Cobley, C. M.; Zeng, J.; Li, W.; Moran, C. H.; Zhang, Q.; Qin, D.; Xia, Y. *Chem. Rev.* **2011**, *111*, 3669.
51. Fleischmann, M.; Hendra, P. J.; McQuillan, A. J. *Chem. Phys. Lett.* **1974**, *26*, 163.
52. Albrecht, M. G.; Creighton, J. A. *J. Am. Chem. Soc.* **1977**, *99*, 5215.
53. Kambhampati, P.; Child, C. M.; Foster, M. C.; Campion, A. *J. Chem. Phys.* **1998**, *108*, 5013.
54. Le Ru, E. C.; Blackie, E.; Meyer, M.; Etchegoin, P. G. *J. Phys. Chem. C* **2007**, *111*, 13794.

55. Nie, S.; Emory, S. R. *Science* **1997**, *275*, 1102.

56. Kneipp, K.; Wang, Y.; Kneipp, H.; Perelman, L. T.; Itzkan, I.; Dasari, R. R.; Feld, M. S. *Phys. Rev. Lett.* **1997**, *78*, 1667.

57. Michaels, A. M.; Jiang; Brus, L. *J. Phys. Chem. B* **2000**, *104*, 11965.

58. Bosnick, K. A.; Jiang, J.; Brus, L. E. *J. Phys. Chem. B* **2002**, *106*, 8096.

59. Futamata, M.; Maruyama, Y.; Ishikawa, M. *Vib. Spectrosc* **2004**, *35*, 121.

60. Futamata, M.; Maruyama, Y.; Ishikawa, M. *J. Phys. Chem. B* **2004**, *108*, 13119.

61. Wilson, R.; Bowden, S. A.; Parnell, J.; Cooper, J. M. *Anal. Chem.* **2010**, *82*, 2119.

62. Sawai, Y.; Takimoto, B.; Nabika, H.; Ajito, K.; Murakoshi, K. *J. Am. Chem. Soc.* **2007**, *129*, 1658.

63. Rao, S.; Raj, S.; Balint, S.; Fons, C. B.; Campoy, S.; Llagostera, M.; Petrov, D. *Appl. Phys. Lett.* **2010**, *96*, 213701.

64. Wang, Y.; Lee, K.; Irudayaraj, J. *J. Phys. Chem. C* **2010**, *114*, 16122.

65. Lim, D.-K.; Jeon, K.-S.; Kim, H. M.; Nam, J.-M.; Suh, Y. D. *Nat. Mater.* **2010**, *9*, 60.

66. Wang, Y.; Wei, H.; Li, B.; Ren, W.; Guo, S.; Dong, S.; Wang, E. *Chem. Commun.* **2007**, 5220.

67. Ni, J.; Lipert, R. J.; Dawson, G. B.; Porter, M. D. *Anal. Chem.* **1999**, *71*, 4903.

68. Hu, J.; Zheng, P.-C.; Jiang, J.-H.; Shen, G.-L.; Yu, R.-Q.; Liu, G.-K. *Anal. Chem.* **2008**, *81*, 87.

69. Hu, J.; Zheng, P.-C.; Jiang, J.-H.; Shen, G.-L.; Yu, R.-Q.; Liu, G.-K. *Analyst* **2010**, *135*, 1084.

70. Braun, G.; Lee, S. J.; Dante, M.; Nguyen, T.-Q.; Moskovits, M.; Reich, N. *J. Am. Chem. Soc.* **2007**, *129*, 6378.

71. Mulvihill, M.; Tao, A.; Benjauthrit, K.; Arnold, J.; Yang, P. *Angew. Chem.-Int.*

Edit. **2008**, *47*, 6456.

72. De Jesús, M. A.; Giesfeldt, K. S.; Sepaniak, M. J. *J. Raman Spectrosc.* **2004**, *35*, 895.
73. Halvorson, R. A.; Vikesland, P. J. *Environ. Sci. Technol.* **2010**, *44*, 7749.
74. Li, X.; Chen, G.; Yang, L.; Jin, Z.; Liu, J. *Adv. Funct. Mater.* **2010**, *20*, 2815.
75. Young, M. A.; Stuart, D. A.; Lyandres, O.; Glucksberg, M. R.; Van Duyne, R. P. *Can. J. Chem.* **2004**, *82*, 1435.
76. Campbell, C. T. *J. Phys. Chem.* **1985**, *89*, 5789.
77. Chimentao, R.; Medina, F.; Sueiras, J.; Fierro, J.; Cesteros, Y.; Salagre, P. *J. Mater. Sci.* **2007**, *42*, 3307.
78. Crossley, M. L. *Ind. Eng. Chem.* **1922**, *14*, 802.
79. John F, C. *Dyes Pigment.* **1999**, *41*, 127.
80. Rode, C. V.; Vaidya, M. J.; Chaudhari, R. V. *Org. Process Res. Dev.* **1999**, *3*, 465.
81. Pradhan, N.; Pal, A.; Pal, T. *Langmuir* **2001**, *17*, 1800.
82. Saha, S.; Pal, A.; Kundu, S.; Basu, S.; Pal, T. *Langmuir* **2009**, *26*, 2885.
83. Rashid, M. H.; Mandal, T. K. *J. Phys. Chem. C* **2007**, *111*, 16750.
84. Lee, C.-L.; Chiou, H.-P.; Syu, C.-M.; Wu, C.-C. *Electrochem. Commun.* **2010**, *12*, 1609.
85. Jena, B. K.; Raj, C. R. *Chem. Eur. J.* **2006**, *12*, 2702.
86. Hrapovic, S.; Liu, Y.; Male, K. B.; Luong, J. H. T. *Anal. Chem.* **2003**, *76*, 1083.
87. Chen, W.; Chen, S. *Angew. Chem. Int. Ed.* **2009**, *48*, 4386.
88. Park, S.; Xie, Y.; Weaver, M. J. *Langmuir* **2002**, *18*, 5792.
89. Rhee, C. K.; Kim, B.-J.; Ham, C.; Kim, Y.-J.; Song, K.; Kwon, K. *Langmuir* **2009**, *25*, 7140.
90. Mayrhofer, K. J. J.; Blizanac, B. B.; Arenz, M.; Stamenkovic, V. R.; Ross, P. N.;

Markovic, N. M. *J. Phys. Chem. B* **2005**, *109*, 14433.

91. Campbell, F. W.; Belding, S. R.; Baron, R.; Xiao, L.; Compton, R. G. *J. Phys. Chem. C* **2009**, *113*, 9053.
92. Bansal, V.; Li, V.; O'Mullane, A. P.; Bhargava, S. K. *CrystEngComm* **2010**, *12*, 4280.
93. Geng, J.; Bi, Y.; Lu, G. *Electrochem. Commun.* **2009**, *11*, 1255.
94. Yuan, J. H.; Wang, K.; Xia, X. H. *Adv. Funct. Mater.* **2005**, *15*, 803.
95. Zhuang, Z.; Su, X.; Yuan, H.; Sun, Q.; Xiao, D.; Choi, M. M. F. *Analyst* **2008**, *133*, 126.
96. Park, S.; Chung, T. D.; Kim, H. C. *Anal. Chem.* **2003**, *75*, 3046.
97. Song, Y.-Y.; Zhang, D.; Gao, W.; Xia, X.-H. *Chem. Eur. J.* **2005**, *11*, 2177.
98. Subhramannia, M.; Ramaiyan, K.; Pillai, V. K. *Langmuir* **2008**, *24*, 3576.
99. Chen, Y.; Schuhmann, W.; Hassel, A. W. *Electrochem. Commun.* **2009**, *11*, 2036.
100. Vidal-Iglesias, F. J.; Solla-Gullón, J.; Rodríguez, P.; Herrero, E.; Montiel, V.; Feliu, J. M.; Aldaz, A. *Electrochem. Commun.* **2004**, *6*, 1080.
101. Zeng, J.; Zhang, Q.; Chen, J.; Xia, Y. *Nano Lett.* **2009**, *10*, 30.
102. Burke, L. D.; Ryan, T. G. *J. Appl. Electrochem.* **1990**, *20*, 1053.
103. Nowicka, A. M.; Hasse, U.; Sievers, G.; Donten, M.; Stojek, Z.; Fletcher, S.; Scholz, F. *Angew. Chem. Int. Ed.* **2010**, *49*, 3006.
104. Koper, M. T. M. *Faraday Discuss.* **2009**, *140*, 11.
105. Demarconnay, L.; Coutanceau, C.; Léger, J. M. *Electrochim. Acta* **2004**, *49*, 4513.
106. Chatenet, M.; Micoud, F.; Roche, I.; Chainet, E. *Electrochim. Acta* **2006**, *51*, 5459.
107. Guo, D. J.; Li, H. L. *Carbon* **2005**, *43*, 1259.
108. Tan, C.; Wang, F.; Liu, J.; Zhao, Y.; Wang, J.; Zhang, L.; Park, K. C.; Endo, M.

Mater. Lett. **2009**, *63*, 969.

109. Blizanac, B. B.; Ross, P. N.; Marković, N. M. *J. Phys. Chem. B* **2006**, *110*, 4735.
110. Marenco, A. J.; Pedersen, D. B.; Wang, S.; Petryk, M. W. P.; Kraatz, H.-B. *Analyst* **2009**, *134*, 2021.
111. Bonfil, Y.; Brand, M.; Kirowa-Eisner, E. *Electroanalysis* **2003**, *15*, 1369.
112. Welch, C. M.; Banks, C. E.; Simm, A. O.; Compton, R. G. *Anal. Bioanal. Chem.* **2005**, *382*, 12.
113. Krista, J.; Kopanica, M.; Novotný, L. *Electroanalysis* **2000**, *12*, 199.
114. Kim, D.; Goldberg, I. B.; Judy, J. W. *Analyst* **2007**, *132*, 350.
115. Fajerwerg, K.; Ynam, V.; Chaudret, B.; Garçon, V.; Thouron, D.; Comtat, M. *Electrochem. Commun.* **2010**, *12*, 1439.
116. Yang, G.-W.; Gao, G.-Y.; Wang, C.; Xu, C.-L.; Li, H.-L. *Carbon* **2008**, *46*, 747.
117. Martin, C. R. *Science* **1994**, *266*, 1961.
118. Martin, C. R. *Acc. Chem. Res.* **1995**, *28*, 61.
119. C. Hulteen, J.; Martin, C. R. *J. Mater. Chem.* **1997**, *7*, 1075.
120. Jessensky, O.; Müller, F.; Gösele, U. *Appl. Phys. A* **1998**, *72*, 1173.
121. Gao, T.; Meng, G.; Zhang, J.; Sun, S.; Zhang, L. *Appl. Phys. A* **2002**, *74*, 403.
122. Tao, G.; et al. *J. Phys.: Condens. Matter* **2002**, *14*, 355.
123. Li, N.; Li, X.; Yin, X.; Wang, W.; Qiu, S. *Solid State Commun.* **2004**, *132*, 841.
124. Wu, Y.; Livneh, T.; Zhang, Y. X.; Cheng, G.; Wang, J.; Tang, J.; Moskovits, M.; Stucky, G. D. *Nano Lett.* **2004**, *4*, 2337.
125. Choi, J.; Sauer, G.; Nielsch, K.; Wehrspohn, R. B.; Gösele, U. *Chem. Mater.* **2003**, *15*, 776.
126. Walter, E. C.; Murray, B. J.; Favier, F.; Kaltenpoth, G.; Grunze, M.; Penner, R. M. *J. Phys. Chem. B* **2002**, *106*, 11407.
127. Braun, E.; Eichen, Y.; Sivan, U.; Ben-Yoseph, G. *Nature* **1998**, *391*, 775.

128. Monson, C. F.; Woolley, A. T. *Nano Lett.* **2003**, *3*, 359.

129. 黃亭凱, 裘性天, 李紫原，電化學法成長金屬奈米材料，國立交通大學應用化學研究所博士論文，民國九十八年

130. Filankembo, A.; Pileni, M. P. *J. Phys. Chem. B* **2000**, *104*, 5865.

131. Pileni, M. P.; Ninham, B. W.; Gulik-Krzywicki, T.; Tanori, J.; Lisiecki, I.; Filankembo, A. *Adv. Mater.* **1999**, *11*, 1358.

132. Hong, B. H.; Bae, S. C.; Lee, C.-W.; Jeong, S.; Kim, K. S. *Science* **2001**, *294*, 348.

133. Sun, Y.; Gates, B.; Mayers, B.; Xia, Y. *Nano Lett.* **2002**, *2*, 165.

134. Sun, Y.; Yin, Y.; Mayers, B. T.; Herricks, T.; Xia, Y. *Chem. Mater.* **2002**, *14*, 4736.

135. Huang, H. H.; Ni, X. P.; Loy, G. L.; Chew, C. H.; Tan, K. L.; Loh, F. C.; Deng, J. F.; Xu, G. Q. *Langmuir* **1996**, *12*, 909.

136. Huang, T.-K.; Cheng, T.-H.; Yen, M.-Y.; Hsiao, W.-H.; Wang, L.-S.; Chen, F.-R.; Kai, J.-J.; Lee, C.-Y.; Chiu, H.-T. *Langmuir* **2007**, *23*, 5722.

137. Huang, T. K.; Lin, K. W.; Tung, S. P.; Cheng, T. M.; Chang, I. C.; Hsieh, Y. Z.; Lee, C. Y.; Chiu, H. T. J. *Electroanal. Chem.* **2009**, *636*, 123.

138. Huang, T.-K.; Chen, Y.-C.; Ko, H.-C.; Huang, H.-W.; Wang, C.-H.; Lin, H.-K.; Chen, F.-R.; Kai, J.-J.; Lee, C.-Y.; Chiu, H.-T. *Langmuir* **2008**, *24*, 5647.

139. Yang, Y.-C.; Huang, T.-K.; Chen, Y.-L.; Mevellec, J.-Y.; Lefrant, S.; Lee, C.-Y.; Chiu, H.-T. *J. Phys. Chem. C* **2011**, *115*, 1932.

140. Yen, M. Y.; Chiu, C. W.; Hsia, C. H.; Chen, F. R.; Kai, J. J.; Lee, C. Y.; Chiu, H. T. *Adv. Mater.* **2003**, *15*, 235.

141. Hsia, C.-H.; Yen, M.-Y.; Lin, C.-C.; Chiu, H.-T.; Lee, C.-Y. *J. Am. Chem. Soc.* **2003**, *125*, 9940.

142. Wang, L. S.; Buchholz, D. B.; Li, Y.; Li, J.; Lee, C. Y.; Chiu, H. T.; Chang, R. P.

H. *Appl. Phys. A* **2007**, *87*, 1.

143. Zhou, Y.; Yu, S. H.; Cui, X. P.; Wang, C. Y.; Chen, Z. Y. *Chem. Mater.* **1999**, *11*, 545.

Chapter 2

Growth of Urchin-like Silver Nanowires by Surfactant-Assisted Galvanic Reductions

2.1 Introduction

In recent years, a lot of researchers are interested in one-dimensional (1D) nanomaterials of noble metal due to their special electrical, optical, and chemical properties, which are different or superior to the bulk ones.[1-3] Among all the noble metal, silver is highly attractive because of the highest electrical and thermal conductivities. Furthermore, silver has the potential of using as active components in catalysis, photography, electronics, photonics, information storage, optoelectronics, biological labeling, imaging, and sensing.[4-7] Therefore, there are a great deal of researches to synthesize silver nanowires (Ag NWs). Until now, various kinds of techniques have been developed such as arc-discharge,[8] template assisted by anoidic aluminum oxide (AAO)[9] or polymer membranes,[10] polyol process,[11,12] seed-mediated growths,[13,14] etc. Here, we report a surfactant assisted synthesis of urchin-like Ag NWs on screen-printed carbon (SPC) electrodes via glavanic reductions of $AgNO_{3(aq)}$ solutions in the presence of cetyltrimethylammonium chloride (CTAC) by Cu foil. We expect the urchin-like Ag NW may find applications in surface-enhanced Raman scattering (SERS) spectroscopy,[15,16] electrochemical sensor for nitrite[17,18] or hydrogen peroxide,[19,20] and antibacterial.[21,22]

2.2 Experimental

2.2.1 Preparation of Growth Substrates

A Cu foil (5 x 5 mm^2) was pre-cleaned with $HCl_{(aq)}$ (Tedia, 0.1 N) for 3 min and rinsed by deionized water. Then, the foil was adhered to a commercial SPC electrode (Zensor R&D SE100, 0.196 cm^2) with conductive silver (Ted Pella). The whole assembly was baked at 353 K in an oven for 30 min.

2.2.2 Preparation of Urchin-like Ag NWs

$AgNO_3$ (Mallinckrodt, 0.064 g, 0.375 mmol) was added to a stirring aqueous solution of CTAC (Taiwan Surfactant, 5.4 x 10^{-3} M, 50 mL) and HNO_3 (Showa, 5 x 10^{-3} M) in a glass beaker. Immediately, the mixture turned white and opaque. After the colloidal suspension was stirred for 15 min, it was allowed to stand for 15 min more. Then, the assembled growth substrate was immersed into the mixture at 303 K for 6 h. After the Cu foil was detached from the electrode, the substrate was rinsed by deionized water. To avoid oxidation, the as-prepared Ag NWs electrodes were stored in a N_2 filled glove box to prevent surface oxidation.

2.2.3 Characterization

The scanning electron microscopic (SEM) and energy dispersive spectroscopic (EDS) data were taken from a Hitachi S-4000 (25 keV) and a JEOL JSM-7401F (15 keV). Transmission electron microscope (TEM) and selected area electron diffraction (SAED) images were captured by a JEOL JEM-2010 at 200 kV. The X-ray diffraction (XRD) patterns were acquired by using a Bruker AXS D8 Advance.

2.3 Results and Discussion

2.3.1 SEM and EDS Characterization

After $AgNO_{3(aq)}$ was added to a stirring solution containing $CTAC_{(aq)}$ and $HNO_{3(aq)}$, the mixture turned white and opaque immediately. This indicated the formation of suspended AgCl colloids. To this mixture, an SPC electrode with a piece

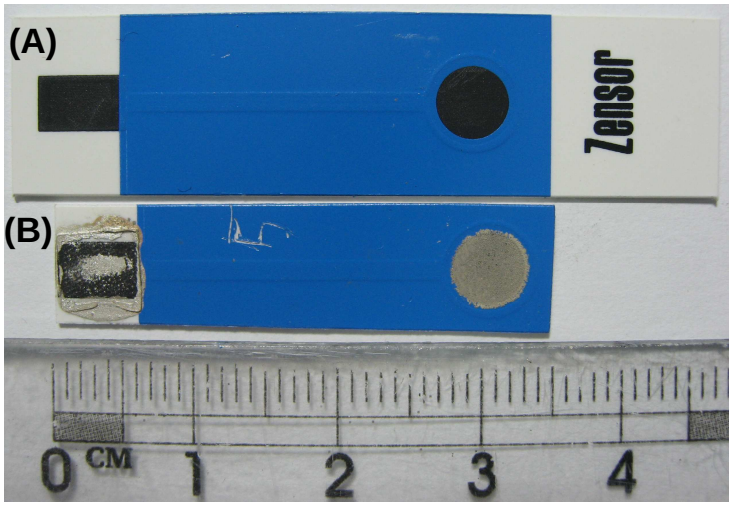

Figure 2.1 Optical images of the commercial SPC electrode (A) before and (B) after the Ag NW growth.

of Cu foil attached to its contact was immersed. The exposed electrode surface turned gray gradually (Figure 2.1). To avoid oxidation, the as-prepared Ag NWs electrodes were stored in a N_2 filled glove box to prevent surface oxidation. In Figure 2.2A, a SEM image shows that the electrode surface is covered by a lot of urchin-like NWs. Based on the EDS measurement displayed in Figure 2.2A (inset), we conclude that the NWs are composed of Ag only. The C signal is assigned to the SPC substrate. From the high magnification image displayed in Figure 2.2B, some branching of the NWs can be observed. The diameters of the NWs are estimated to be about 100 nm while the lengths are found to be in the range 3 – 10 μm. With different growth conditions, the diameters can vary from 80 to 120 nm while the lengths can differ from 1 to 10 μm. An individual cluster of NWs formed initially at 2 h (Figure 2.3) show that many NWs protruded from a surface on the substrate to form the urchin-like morphology. The side-view image is shown in Figure 2.2C. We can notice that whole urchin-like Ag NWs arise from the electrode surface. The image displays that in each urchin-like structure, the NWs radiate from an apparent common nucleus. Other growth conditions of different Ag samples are shown in appendix.

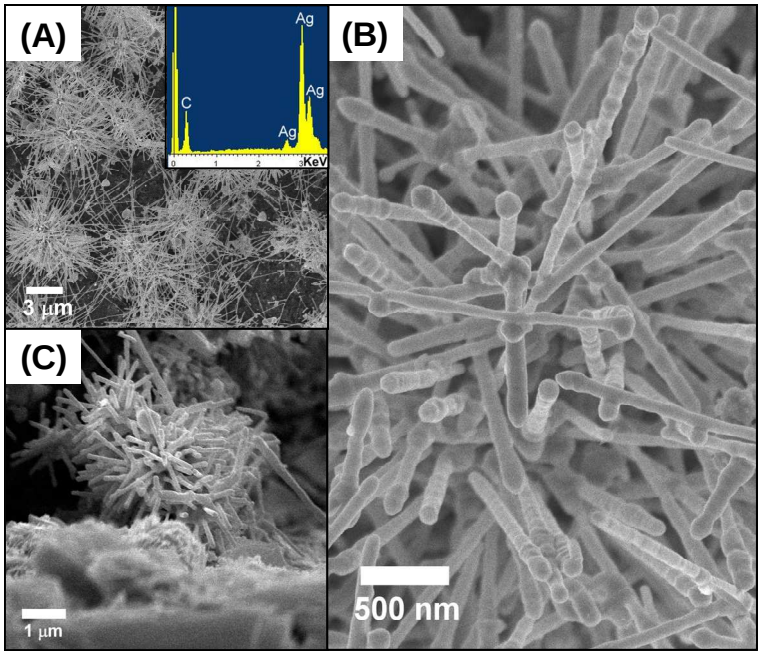

Figure 2.2 SEM studies of urchin-like Ag NWs on a SPC electrode. (A) Low magnification surface image (inset, EDS of an area in (A)), (B) high magnification image, and (C) high magnification side-view image.

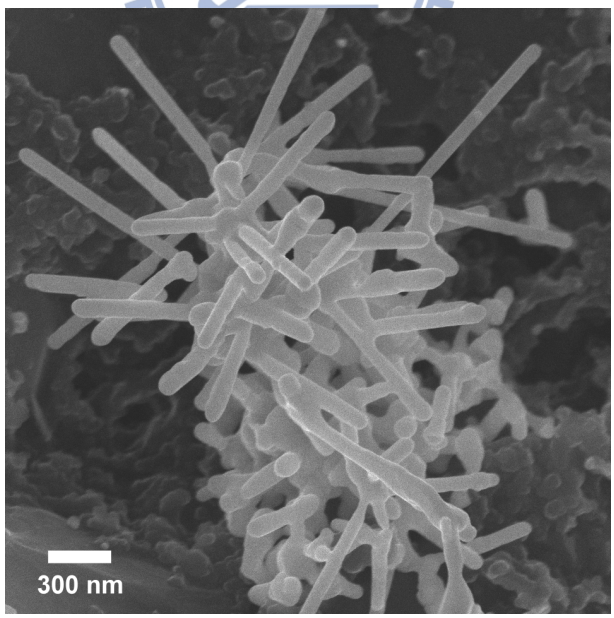

Figure 2.3 A cluster of urchin-like Ag NWs formed initially on a SPC electrode at 2 h.

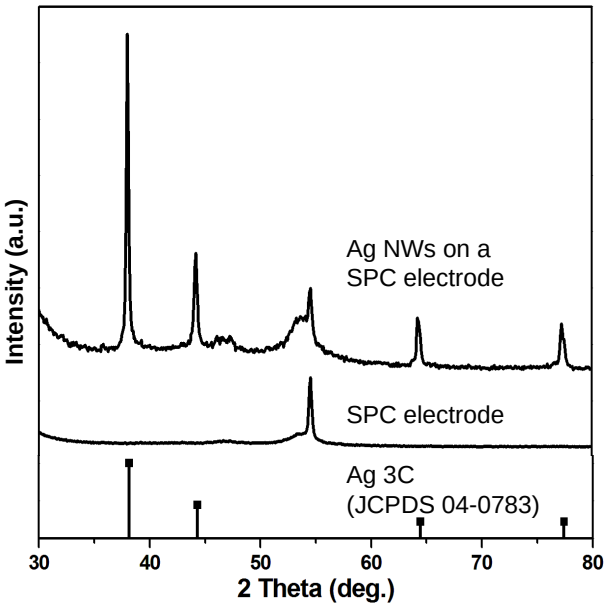

Figure 2.4 XRD pattern of Ag NWs on a SPC electrode.

2.3.2 XRD Analysis

The XRD patterns are shown in Figure 2.4. The peaks at 2θ=38.1°, 44.3°, 64.5°, 77.4° are assigned to Ag (111), (200), (220), and (311) reflections, respectively (JCPDS file 04-0783).[23] The broad band around 54° comes from the SPC electrode. From the patterns, the lattice parameter *a* was estimated to be 0.409 nm, consistent with the value reported for Ag.[23]

2.3.3 TEM Characterization

TEM studies of a group of urchin-like NWs are shown in Figure 2.5. The image in Figure 2.5A reveals an overall morphology closely related to the ones presented in Figure 2.2C and Figure 2.3. Extension of the NWs from an apparent initial growth point and branching of some NWs are observed. The SAED patterns of the tip and the root of a NW, which branches from another NW stem, are shown in Figure 2.5B and 2.5C, respectively. Interestingly, they display the same set of dot patterns revealing their single crystalline nature. They both correspond to the [001] crystallographic zone axis of an fcc structure with the lattice parameter *a* calculated to be 0.41 nm.[23]

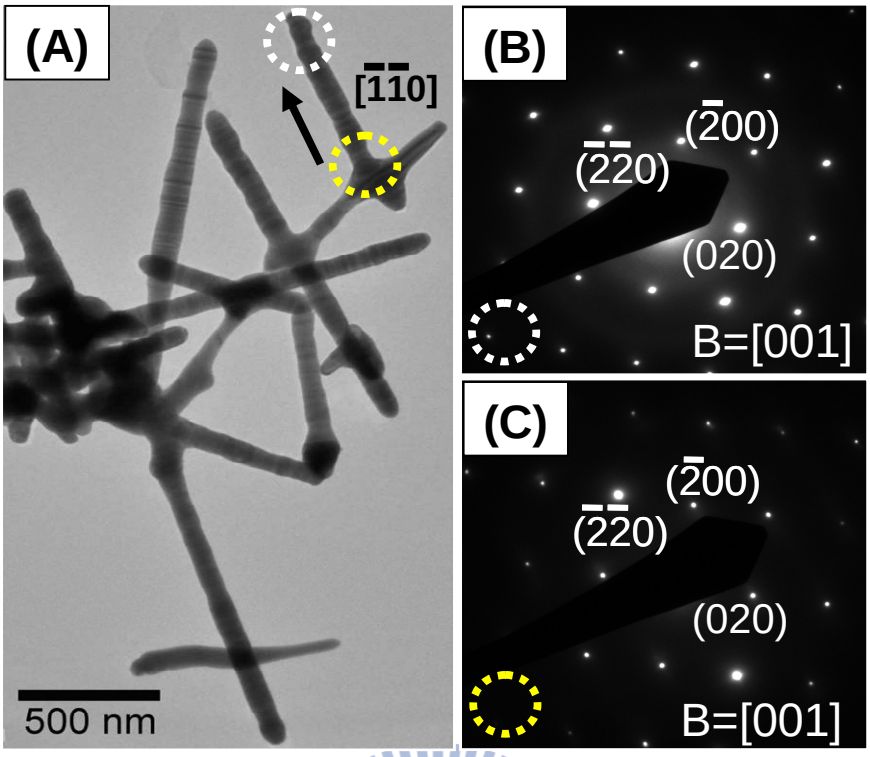

Figure 2.5 (A) TEM image of urchin-like Ag NWs. SAED patterns from (B) the white-dashed and (C) the yellow-dashed circles in (A).

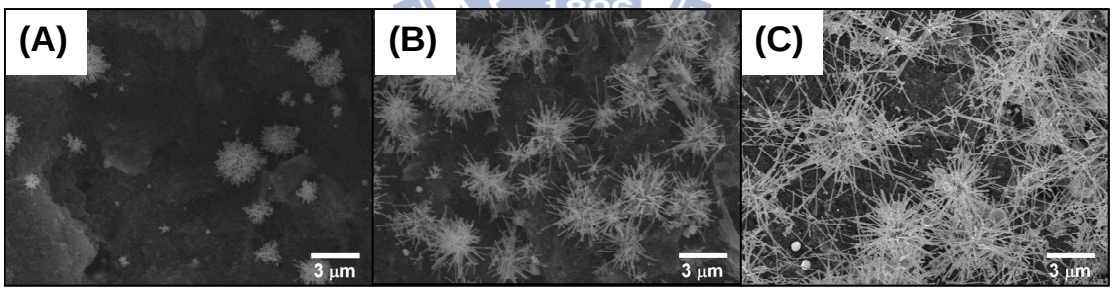

Figure 2.6 Effect of lengths of growth time. SEM images of urchin-like Ag NWs grown for (A) 1 h, (B) 3 h, and (C) 6 h.

The NW growth direction is determined to be along the [-1-10] direction. The data suggest that the overall branched Ag NW structure is a single crystal.

2.3.4 Reaction Time Influence

SEM images of urchin-like Ag NWs grown from different lengths of time were shown in Figure 2.6. At 1 h, there were few urchin-like NWs with lengths less than 1

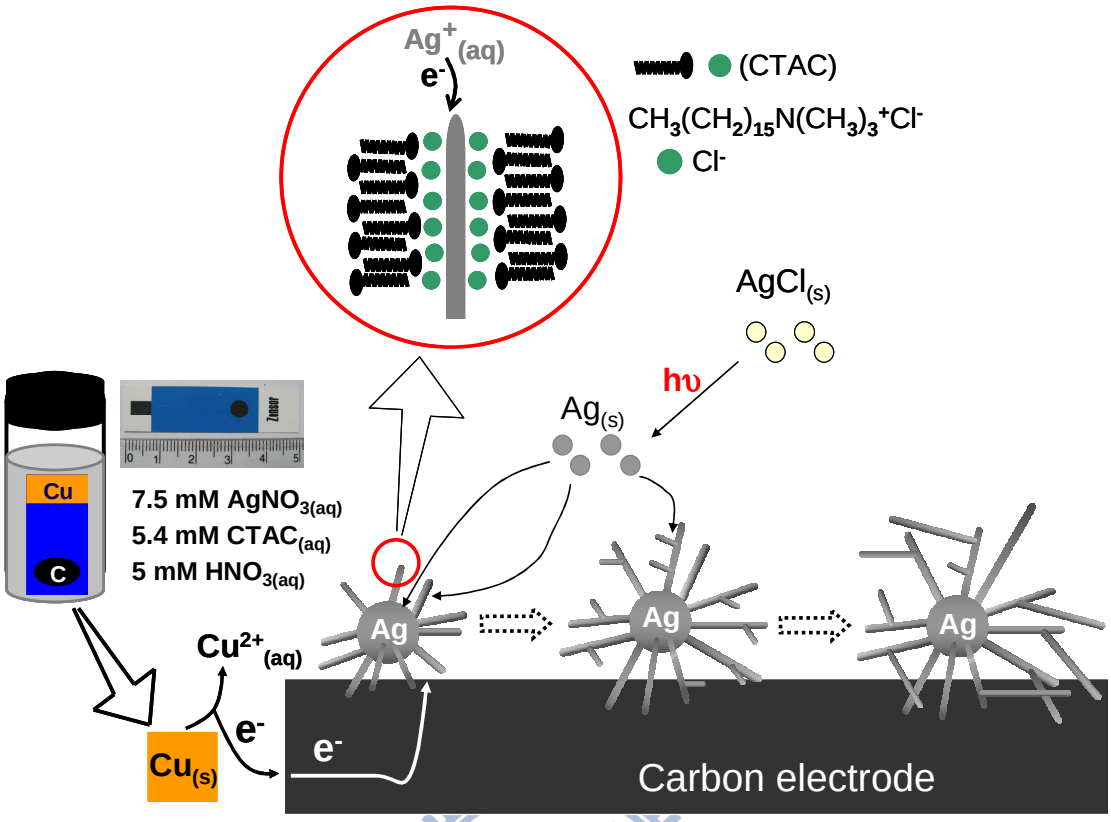

Figure 2.7 Proposed mechanism of urchin-like Ag nanowire.

μm on the SPC electrode (Figure 2.6A). At 3 h, more urchin-like clusters with longer NWs were observed, as shown in Figure 2.6B. When the growth was extended to 6 h, more coverage of longer NWs on the electrode surface was found in Figure 2.6C.

2.3.5 Proposed Growth Mechanism

We suggest that our previously proposed growth pathways for one-dimensional Cu, Ag, and Au nanostructures are applicable for the urchin-like Ag NWs too.[13,24-26] The preparation of Ag NW is dependent on the presence of CTAC and HNO_3. All the growth process is presented in Figure 2.7. At the beginning, there are 7.5 mM $Ag^+_{(aq)}$ ions in this reaction solution. Some $Ag^+_{(aq)}$ ions (2.1 mM) would reduce by $Cu_{(s)}$ to form $Ag_{(s)}$ clusters through the galvanic reduction, $2Ag^+_{(aq)} + Cu_{(s)} \rightarrow 2Ag_{(s)} + Cu^{2+}_{(aq)}$ $E° = 0.46$ V.[27] The clusters enlarged as more Ag(s) reduced to become urchin nucleus on the electrode. At the same time, the other $Ag^+_{(aq)}$ ions (5.4 mM) combined with

$Cl^-_{(aq)}$ anions (5.4 mM) from CTAC molecules to form $AgCl_{(s)}$ colloids which covered by a shell of CTAC molecules. Since the reaction $2AgCl_{(s)} + Cu_{(s)} \rightarrow 2Ag_{(s)} + Cu^{2+}_{(aq)} + 2Cl^-_{(aq)}$ $E° = -0.12$ V[27] is not thermodynamically favored, the source of Ag cannot obtained via this route. The growth cannot just proceed via the reaction $2Ag^+_{(aq)} + Cu_{(s)} \rightarrow 2Ag_{(s)} + Cu^{2+}_{(aq)}$ without CTAC either because this reaction alone did not produce the urchin-like NWs structure. As the literature reports, it is known that $AgCl_{(s)}$ can be reduced to $Ag_{(s)}$ by light.[28] The $Ag_{(s)}$ clusters reduced by light could be seeds randomly adsorbed on the urchin nucleus and initiated the growth of Ag NWs assisted by CTAC as the surface capping reagent, which may selectively adsorbed on low-index facets to form a bilayer interface structure.[29,30] The presence of $NO_3^-{}_{(aq)}$ ions in the growth solution is another determinant for controlling the crystal shape in the system. The function of the ions may oxidize $Ag_{(s)}$ into $Ag^+_{(aq)}$ ions. During the crystal growth, the less stable facets might be oxidized by $NO_3^-{}_{(aq)}$ easily, leaving the more stable facets exposed for further developments. As a result, all these factors function cooperatively in the reaction to direct the crystals to grow into urchin-like Ag NWs.

2.3.6 Extensive Application on Electrochemical Deposition

In our reaction, reduction of $Ag^+_{(aq)}$ ions were contributed by galvanic reductions. However, we discovered that Ag NWs could be grown direct on Au or Pt seeding layers on Indium Tin Oxide (ITO) substrate via a simple two-electrode electrochemical deposition method in the same reaction solution at 293 K. The results are shown in Figure 2.8. Figure 2.8A to 2.8D display that there are some Ag NWs on the ITO substrates. The diameters are about 60 nm, which are smaller than the ones react by galvanic reductions. The lengths are found to be in the range 1 – 5 μm. Based on the EDS measurement displayed in Figure 2.8A (inset) and 2.8C (inset), we

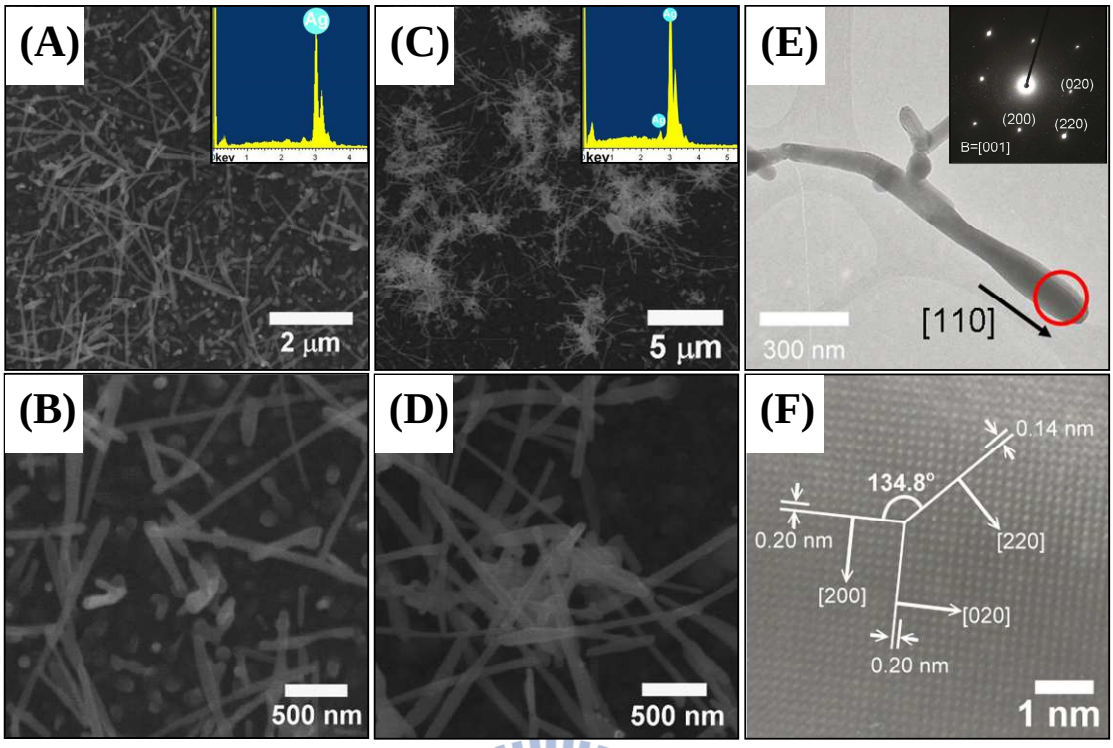

Figure 2.8 SEM images of Ag NWs on ITO substrates with different kinds seeding laeyer. On Au seeding layer (A) Low magnification surface image (inset, EDS of an area in (A)), (B) high magnification surface image. On Pt seeding layer (C) Low magnification surface image (inset, EDS of an area in (C)), (D) high magnification surface image. (E) TEM image of Ag NWs in (C) (inset, [001] zone SAED of the Ag NW) (F) HRTEM image of the red marked circle region in (E).

conclude that the NWs are composed of Ag only. TEM characterizations are displayed in Figure 2.8E and 2.8F. The SAED pattern in Figure 2.8E (inset) shows a spot pattern, which can be indexed to be [001] zone axis of Ag reveals that the Ag NW is single crystalline. From the pattern, the growth direction of Ag NW is determined to be along [110] direction, which is identical to the one reacted by galvanic reduction. Figure 2.8F presents an HRTEM image from the red marked circle region in Figure 2.8E. The dihedral angle between [220] and [200] is 134.8°, which is close to the theoretical value of an fcc structure. The [220] and [200] d-spacing are measured to be

0.14 nm and 0.20 nm, respectively. Both the value are close to the previous report of Ag, 0.144 nm and 0.204 nm.[23]

2.4 Conclusion

In summary, we have developed a simple low-cost surfactant-assisted galvanic reduction process to grow urchin-like Ag NWs on SPC electrodes. Both CTAC and HNO_3 molecules are essential ingredients to shape the urchin-like Ag NW. Moreover, we can use electrochemical deposition to synthesize Ag NW on Au or Pt seeding layers on ITO substrates with similar reaction condition.

2.5 References

1. Favier, F.; Walter, E. C.; Zach, M. P.; Benter, T.; Penner, R. M. *Science* **2001,** *293*, 2227.
2. Cui, Y.; Wei, Q.; Park, H.; Lieber, C. M. *Science* **2001,** *293*, 1289.
3. Sung-Wook, C.; Jae-Young, Y.; Heath, J. R. *Appl. Phys. Lett.* **2000,** *76*, 2068.
4. Hoelderich, W. F. *Catal. Today* **2000,** *62*, 115.
5. Challener, W. A.; Ollmann, R. R.; Kam, K. K. *Sens. Actuator B:Chem.* **1999,** *56*, 254.
6. Jin, R.; Cao, Y.; Mirkin, C. A.; Kelly, K. L.; Schatz, G. C.; Zheng, J. G. *Science* **2001,** *294*, 1901.
7. Gould, I. R.; Lenhard, J. R.; Muenter, A. A.; Godleski, S. A.; Farid, S. *J. Am. Chem. Soc.* **2000,** *122*, 11934.
8. Zhou, Y.; Yu, S. H.; Cui, X. P.; Wang, C. Y.; Chen, Z. Y. *Chem. Mater.* **1999,** *11*, 545.
9. Choi, J.; Sauer, G.; Nielsch, K.; Wehrspohn, R. B.; Gösele, U. *Chem. Mater.* **2003,** *15*, 776.
10. Martin, B. R.; Dermody, D. J.; Reiss, B. D.; Fang, M.; Lyon, L. A.; Natan, M. J.; Mallouk, T. E. *Adv. Mater.* **1999,** *11*, 1021.
11. Sun, Y.; Xia, Y. *Adv. Mater.* **2002,** *14*, 833.
12. Sun, Y.; Gates, B.; Mayers, B.; Xia, Y. *Nano Lett.* **2002,** *2*, 165.
13. Murphy, C. J.; Jana, N. R. *Adv. Mater.* **2002,** *14*, 80.
14. Jana, N. R.; Gearheart, L.; Murphy, C. J. *Chem. Commun.* **2001**, 617.
15. Nie, S.; Emory, S. R. *Science* **1997,** *275*, 1102.
16. Wang, H. H.; Liu, C. Y.; Wu, S. B.; Liu, N. W.; Peng, C. Y.; Chan, T. H.; Hsu, C. F.; Wang, J. K.; Wang, Y. L. *Adv. Mater.* **2006,** *18*, 491.
17. Gao, P.; Zhang, M.; Hou, H.; Xiao, Q. *Mater. Res. Bull.* **2008,** *43*, 531.

18. Krista, J.; Kopanica, M.; Novotný, L. *Electroanalysis* **2000,** *12*, 199.

19. Welch, C. M.; Banks, C. E.; Simm, A. O.; Compton, R. G. *Anal. Bioanal. Chem.* **2005,** *382*, 12.

20. Yonghai, S.; Kang, C.; Li, W.; Shouhui, C. *Nanotechnol.* **2009,** *20*, 105501 (8 pp.).

21. Chi, G. J.; Yao, S. W.; Fan, J.; Zhang, W. G.; Wang, H. Z. *Surf. Coat. Technol.* **2002,** *157*, 162.

22. Sondi, I.; Salopek-Sondi, B. *J. Colloid Interface Sci.* **2004,** *275*, 177.

23. Joint Committee for Power Diffraction (JCPDS) File No. 04-0783, International Center for Diffraction Data (ICDD), 1982.

24. Huang, T.-K.; Cheng, T.-H.; Yen, M.-Y.; Hsiao, W.-H.; Wang, L.-S.; Chen, F.-R.; Kai, J.-J.; Lee, C.-Y.; Chiu, H.-T. *Langmuir* **2007,** *23*, 5722.

25. Huang, T.-K.; Chen, Y.-C.; Ko, H.-C.; Huang, H.-W.; Wang, C.-H.; Lin, H.-K.; Chen, F.-R.; Kai, J.-J.; Lee, C.-Y.; Chiu, H.-T. *Langmuir* **2008,** *24*, 5647.

26. Yang, Y.-C.; Huang, T.-K.; Chen, Y.-L.; Mevellec, J.-Y.; Lefrant, S.; Lee, C.-Y.; Chiu, H.-T. *J. Phys. Chem. C* **2011,** *115*, 1932.

27. Bard, A. J.; Faulkner, L. R. *Electrochemical Methods: Fundamentals and Applications*; John Wiley & Sons: New York, **1980**.

28. Zayat, M.; Einot, D.; Reisfeld, R. *J. Sol-Gel Sci. Technol.* **1997,** *10*, 67.

29. Nikoobakht, B.; El-Sayed, M. A. *Langmuir* **2001,** *17*, 6368.

30. Gao, J.; Bender, C. M.; Murphy, C. J. *Langmuir* **2003,** *19*, 9065.

Chapter 3

Surface Enhanced Raman Scattering Imaging of a Single Molecule on Urchin-like Silver Nanowires

3.1 Introduction

Since surface enhanced Raman scattering (SERS) was first observed by Fleischman et al. in 1974[1], fundamental research and practical application based on this powerful technique for detecting a minute quantity of molecules are intensively studied in recent years. Two mechanisms are often mentioned in the literature to explain the SERS phenomenon. The primary one is the electromagnetic effect and the second one is the charge-transfer effect.[2,3] Since silver shows superior SERS performance, various silver nanostructures, such as nanoparticle (NP),[4] nanowire (NW),[5,6] nanorod (NR),[7] nanoplate,[8] and nanodendrite,[9-13] have been investigated as highly sensitive substrates. A lot of methods to synthesize these nanostructures have been developed. These include photochemical processes,[14,15] seed-mediated growths,[16,17] hard template assisted growths,[18] and galvanic displacement reactions.[19] Due to their overall morphology, lots of SERS hot spots, created from gaps, slits, vacancies, and crossovers, are provided.[20-24] In general, the SERS performance correlates highly to the amount of hot spots. Since 1997, detecting single molecules of Rhodamine 6G (R6G), DNA, and pathogens adsorbed on Ag NPs and metal nanostructures with designed nanogaps by SERS have been reported.[25-35] Recently, we have reported the growths of one-dimensional (1D) Ag,[36-38] Cu,[38] and Au[39,40] nanostructures via several heterogeneous reactions. We discover that surfactant assisted galvanic reductions provide low cost, one step, and near room temperature

growth routes to these nanosized 1D metals. By using this strategy, here, we demonstrate the growth of urchin-like Ag NWs on screen-printed carbon (SPC) electrodes. We discover that the Ag NW substrate shows superior SERS performance and is able to detect a single R6G molecule by Raman image mapping. Our findings are discussed below.

3.2 Experimental

3.2.1 Preparation of Urchin-like Ag NWs

An SPC electrode with a pre-cleaned Cu foil attached was immersed into a reaction solution (50 mL), which contained $AgNO_3$ (0.064 g, 0.375 mmol), CTAC (0.89 M, 0.3 mL) and HNO_3 (0.312 M, 0.8 mL) in a glass beaker for 6 h. Then, the SPC electrode was rinsed by deionized water and stored in a N_2 filled glove box to avoid oxidation. More detail information for synthesizing urchin-like Ag NWs was described in chapter 2.2.

3.2. Characterizations and Spectroscopic Measurements

The scanning electron microscopic (SEM) and energy dispersive spectroscopic (EDS) data were taken from a Hitachi S-4000 (25 keV) and a JEOL JSM-7401F (15 keV). The UV-Vis absorption spectra of the Ag NWs, removed from the electrodes and dispersed in ethanol by sonication, were taken from a spectrophotometer (Hitachi 3010 double-beam UV-visible spectrometer). The Raman spectra were acquired using a high resolution confocal Raman spectrometer (HORIBA LabRAM HR800, excitation wavelength 532 nm) and a potable Raman (MiniRam™ II Raman Spectrometer System, excitation wavelength 785 nm). R6G (Sigma-Aldrich) dissolved in pure ethanol (Sigma-Aldrich, purity > 99.5 %) were chosen to be the probe molecule in the analytes in the experiments. R6G (10 μL) with various concentrations were dropped on the Ag NWs SPC substrates for the measurements. The spectra measured sequentially using the same instrumental settings were

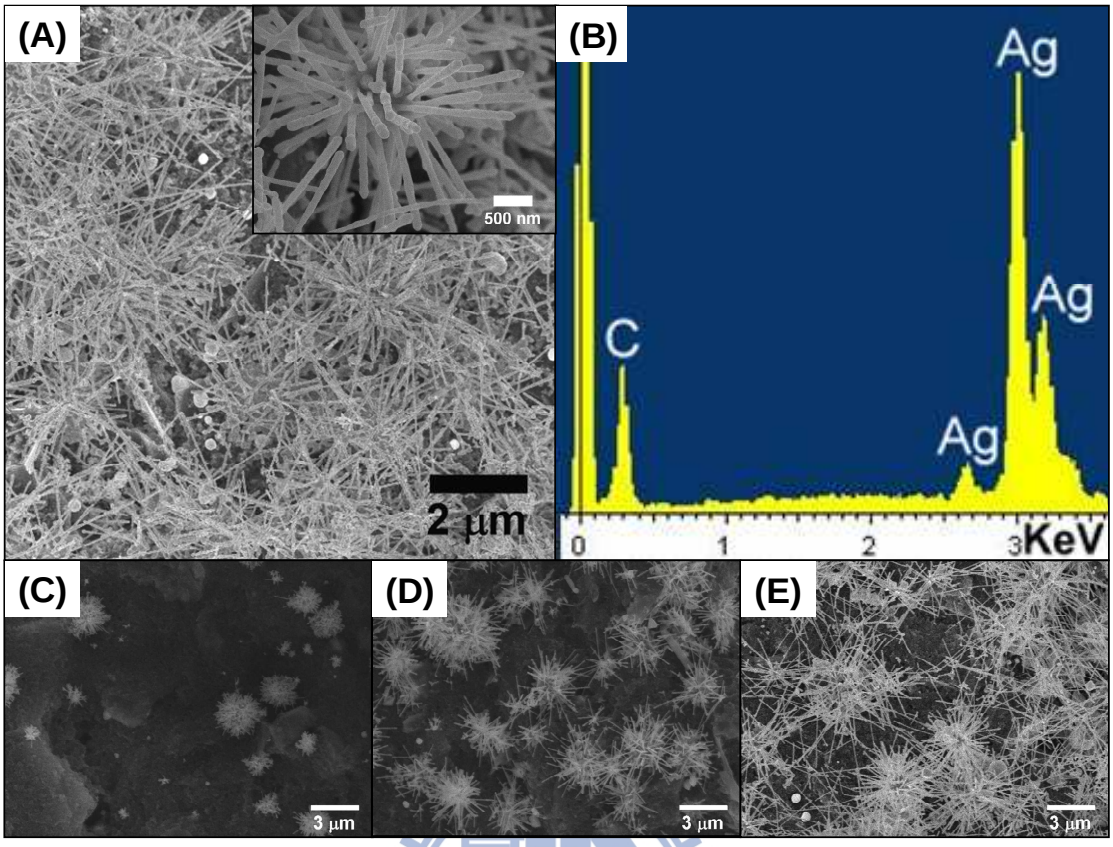

Figure 3.1 SEM studies of urchin-like Ag NWs on a SPC electrode (A) Low magnification surface image (inset, high magnification of a single cluster of urchin-like Ag NWs) (B) EDS of an area in (A). SEM images of urchin-like Ag NWs grown for (C) 1 h, (D) 3 h, and (E) 6 h.

compared. Raman mapping studies (excitation wavelength 532 nm) were carried out for the samples on an XY-stage. For each Raman mapping study of an area 3600 μm^2 (60 x 60 μm^2), 441 points (21 x 21 points) were collected.

3.3 Results and Discussion

3.3.1 SEM and EDS Characterizations

Figure 3.1A displays that there are lots of urchin-like Ag NWs on an SPC electrode. Inset of Figure 3.1A shows a single urchin-like structure of Ag. Based on the EDS measurement, we suppose that the NWs are composed of Ag only. Urchin-like Ag NWs grown at different time are illustrated in Figure 3.1 C to Figure

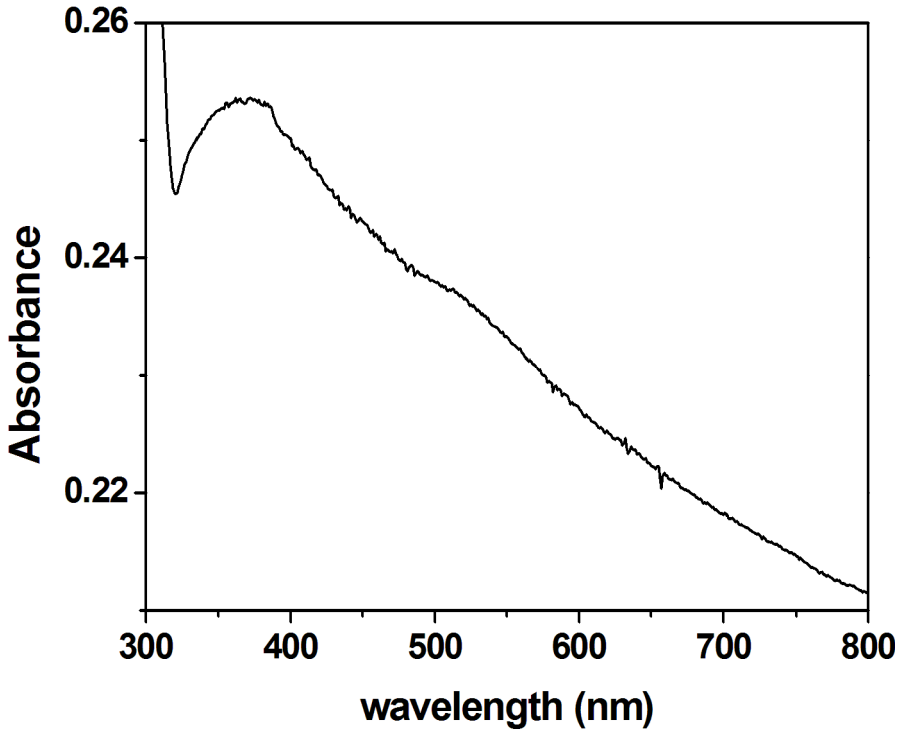

Figure 3.2 UV-visible absorption spectrum of urchin-like Ag NWs.

3.1E. We discover that both the amount of urchin-like cluster and the length of NW are increasing with the reaction time.

3.3.2 UV-visible Analysis

Figure 3.2 shows a typical UV-visible absorption spectrum of the urchin-like Ag NWs suspended in ethanol. The absorption peak at ca. 380 nm was attributed to the plasmon response from the transverse mode of the NWs while the broad band extended from 500 nm was assigned to the longitudinal modes of the NWs with different aspect ratios.[41] The shoulder at 350 nm was commonly observed for long Ag NWs.

3.3.2 SERS Analysis

Correlations between SERS and surface plasmon resonance (SPR) have been studied and connected both theoretically and experimentally.[42-44] It has been proved that optimizing the correlation between the SPR of the substrate and the excitation

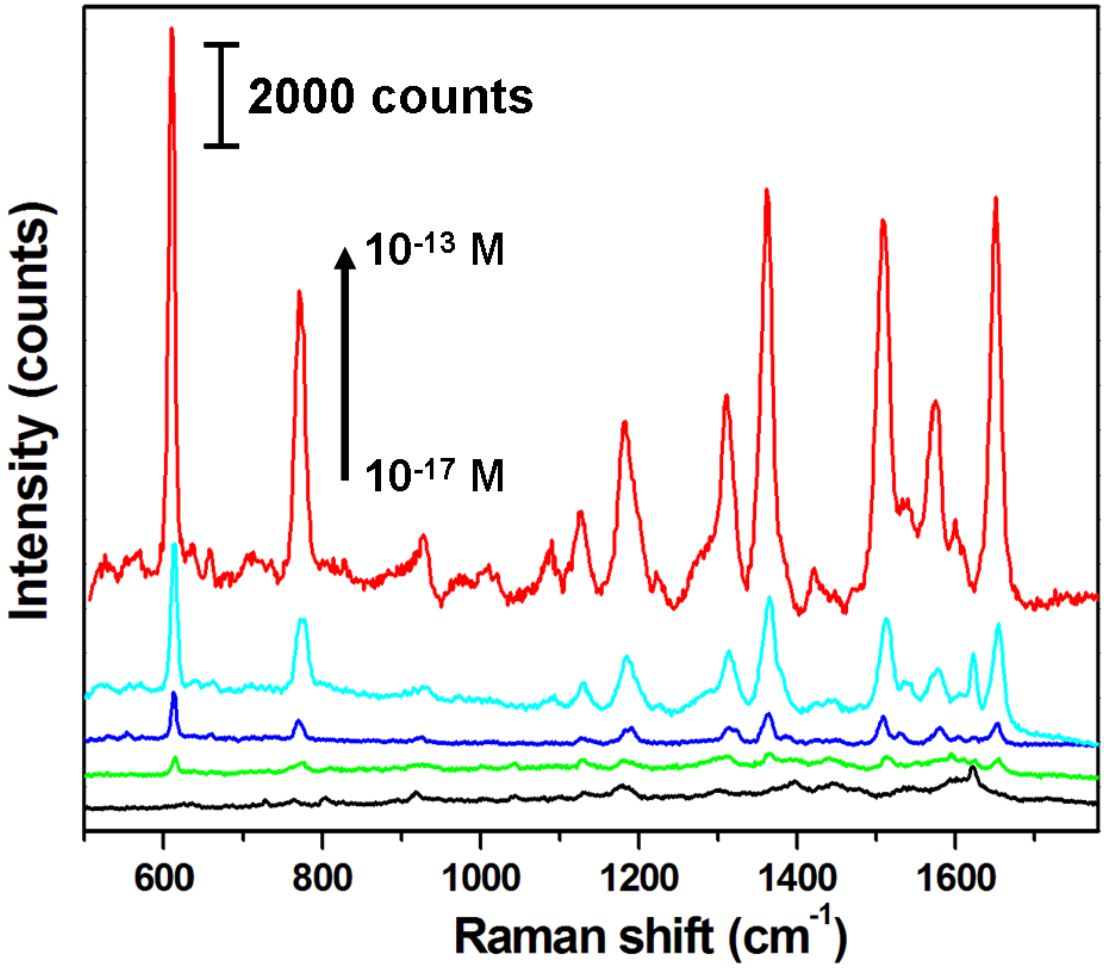

Figure 3.3 SERS (Excitation: 532 nm, power: 5 mW, data collection: 5 s) of R6G (10 μL, in ethanol) on the urchin-like Ag NWs. The R6G concentrations are 10^{-13} M (red), 10^{-14} M(cyan), 10^{-15} M (blue), 10^{-16} M (green), and 10^{-17} M (black).

wavelength provides an efficient way to increase SERS performance.[45] Since R6G has large Raman scattering cross section at 532 nm,[46] which is near the longitudinal modes of the NWs. The excitation wavelength of 532 nm was applied for the SERS experiments discussed below. In Figure 3.3, the vibration signals from R6G (10^{-13} - 10^{-17} M) on a urchin-like Ag NW on SPC substrate (with a growth time 6 h) can be observed clearly by Raman. Assignments to specific vibrational modes were listed in Table 3.1.[47,48] As the concentration decreases, the SERS signal intensities decrease accordingly. Yet, the signals are still visible even at the concentration as low as 10^{-16}

Table 3.1 Assignments of Raman frequencies of R6G in the spectra.

Frequency (cm^{-1})	Assignments
614	ip XRD, op XRD
776	op C-H bend, ip XRD
1127	ip C-H bend
1184	ip XRD, C-H bend, N-H bend
1309	ip XRB, N-H bend, CH2 wag
1366	XRS, ip C-H bend
1509	XRS, C-N str, C-H bend, N-H bend
1650	XRS, ip C-H bend

ip: in plane, op: out of plane, XRD: xanthene ring deformations, XRB: xanthene ring breath, XRS: xanthene ring stretch, str: stretch.

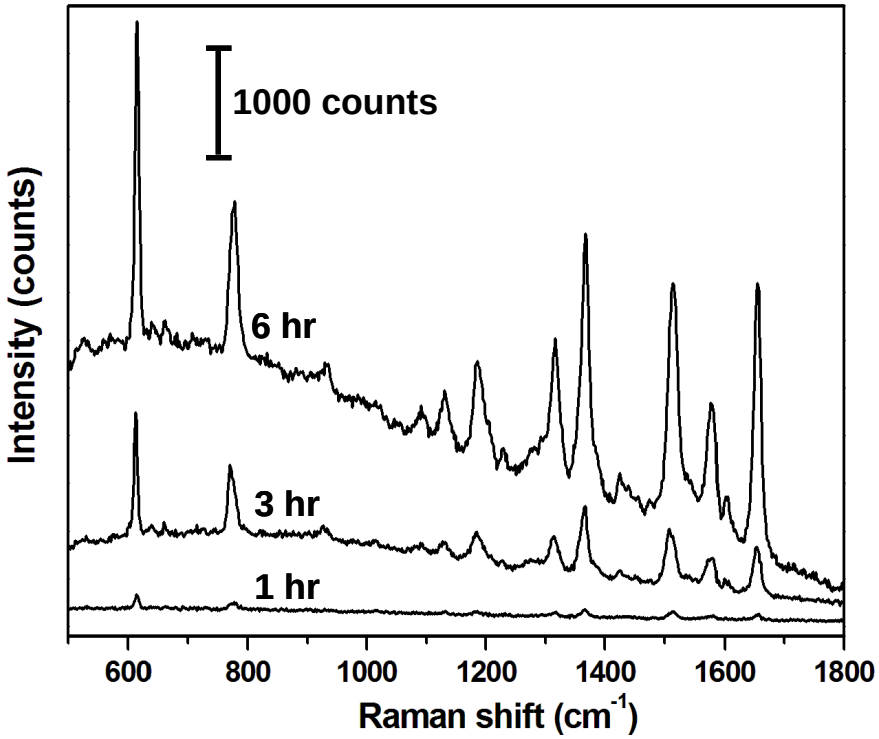

Figure 3.4 Raman spectra of R6G (1 μM, 10 μL, in ethanol) on urchin-like silver NWs with different growth time periods. (Excitation: 532 nm, power: 0.05 mW, data collection: 1 s)

Table 3.2 Reported detection limits and Analytical Enhancement Factors (AEF) of R6G on different substrates.

Substrate	Detection Limit of R6G (M)	Analytical Enhancement Factor	Ref
Ag nanocrystals on Si	10^{-8}	10^{5}	49
Ag NPs on glassy carbon	10^{-9}	-[b]	50
Au-coated ZnO NRs	10^{-9}	10^{6}	51
Au flowerlike nanoarchitectures	10^{-12}	-[b]	52
Ag NR arrays on Si	10^{-14}	-[b]	53
Ag NPs-coated Si NWs	10^{-14}	2.3×10^{8}	54
Roughened Ag substrate	2×10^{-15}	-[b]	55
Ag nanodesert roses on Si	10^{-15}	2×10^{10}	56
Ag and Au NPs containing substrates	10^{-16}	-[b]	57
Ag urchin-like NWs on SPC	10^{-16}	10^{13}	**This study**

a NP: nanoparticle, NR: nanorod, NW: nanowire, SPC: screen-printed carbon.

b Not reported.

M. To our knowledge, this is one of the lowest detectable R6G concentration reported so far (See Table 3.2 for other examples).[49-57] When the growth time was shortened,

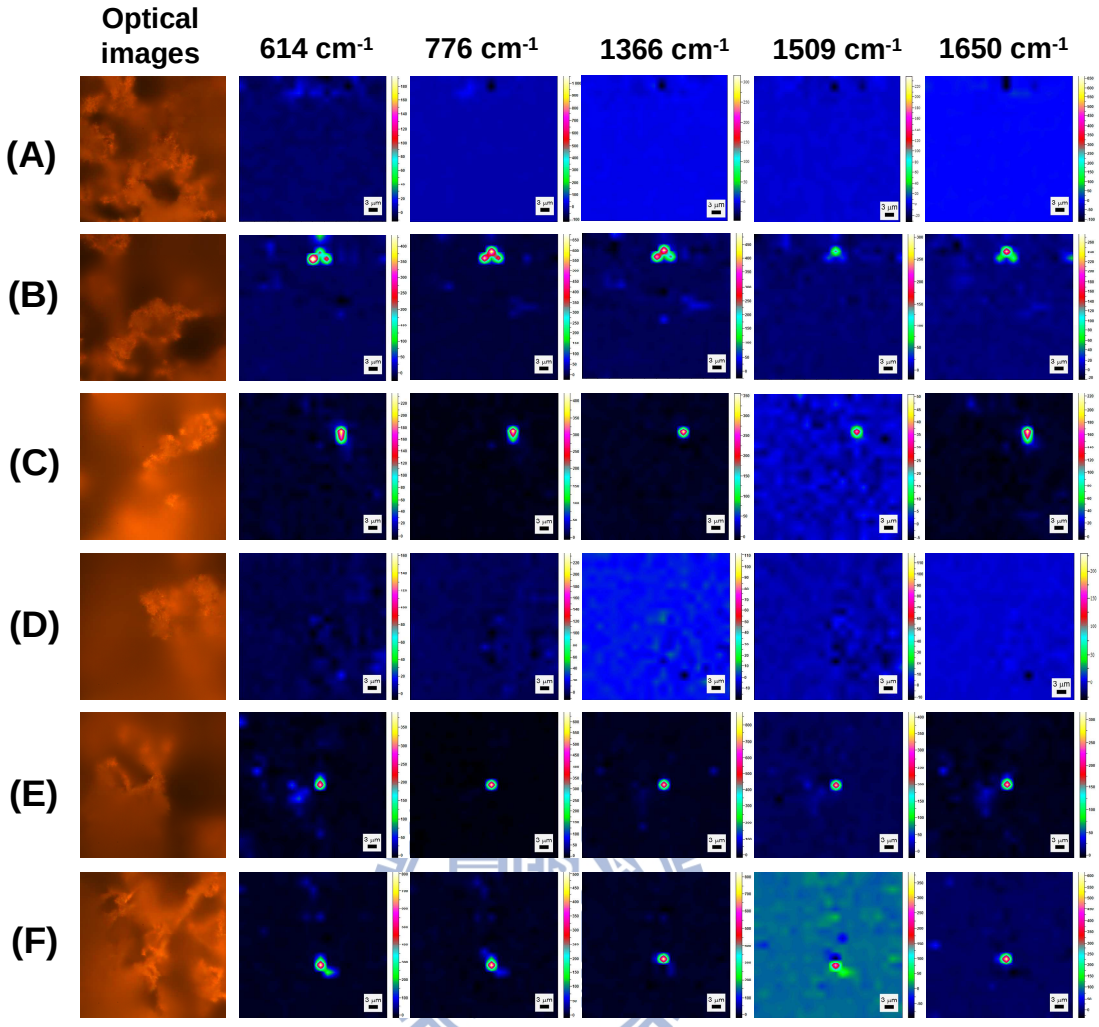

Figure 3.5 Images of randomly selected areas (60 μm x 60 μm) of urchin-like Ag NWs on a SPC electrode. Series (A) - (F), optical images and corresponding Raman mappings of the R6G signals at 614 cm^{-1}, 776 cm^{-1}, 1366 cm^{-1}, 1509 cm^{-1}, and 1650 cm^{-1}.

short and thin Ag NWs were obtained on the substrates (Figure 3.1CDE). The enhancement capability diminished drastically too (Figure 3.4). This can be rationalized by the following reasons. As we know, the SERS effect correlates extensively to the electric magnetic field enhancement by the so-called “hot-spots”. In the urchin-like Ag NWs fabricated in this study, SERS hot-spots may originate from metal gaps, slits, vacancies and crossovers.[20-24,40] Short and sparse Ag NWs would

create few gaps, slits, and vacancies. Consequently, these substrates showed much inferior enhancement performance.

To demonstrate the capability of the urchin-like Ag NWs in sensing R6G further, the following SERS mapping studies was carried out. We estimate that about 6000 R6G molecules exist on the urchin-like Ag NW on an SPC substrate when R6G (1 fM, 10 μL) is applied. Since the substrate has a surface area 0.196 cm^2, we can determine that there are only thirty R6G molecules on an area 10^6 μm^2. Thus, we anticipate locating only a single R6G molecule in a mapped-area 3600 μm^2 (60 x 60 μm^2). By using the Ag NWs, the Raman mappings of R6G peaks at 614 cm^{-1}, 776 cm^{-1}, 1309 cm^{-1}, 1366 cm^{-1}, 1509 cm^{-1}, 1650 cm^{-1} are displayed in Figure 3.5. From six randomly selected areas (60 x 60 μm^2 each) on the substrate, six sets of R6G signals are observed in four areas. Among them, one area displayed in the series B in Figure 3.5, a cluster of three sets of R6G signals is shown. In series C, E, F, each image displays only a single signal at the same point within the mapped-area 3600 μm^2. On the other hand, two areas (A and D) are totally silent from any R6G response. This means that no R6G molecules exist in these two areas. Since the R6G molecules were randomly adsorbed on the substrate, the observation agrees with the estimated R6G density on the surface. That is on average, one molecule was adsorbed on each of the mapped areas. We conclude that each set of SERS mapping data were generated by a single R6G molecule. The Raman spectra of the single R6G molecule signals in Figure 3.5 are displayed in Figure 3.6. Further investigations of time-resolved surface-enhanced Raman spectra are shown in Figure 3.7. As the table in Figure 3.7 displayed, Raman peaks at 1658 cm^{-1}, 1516 cm^{-1}, 1314 cm^{-1}, 1368 cm^{-1}, and 1098 cm^{-1} are changed in both wavelength and intensity. In literature, it is found that the orientation of molecules on the surface affects the Raman intensities of specific vibrational modes strongly.[58] This is because certain modes, such as in-plane and out-of-plane vibrations,

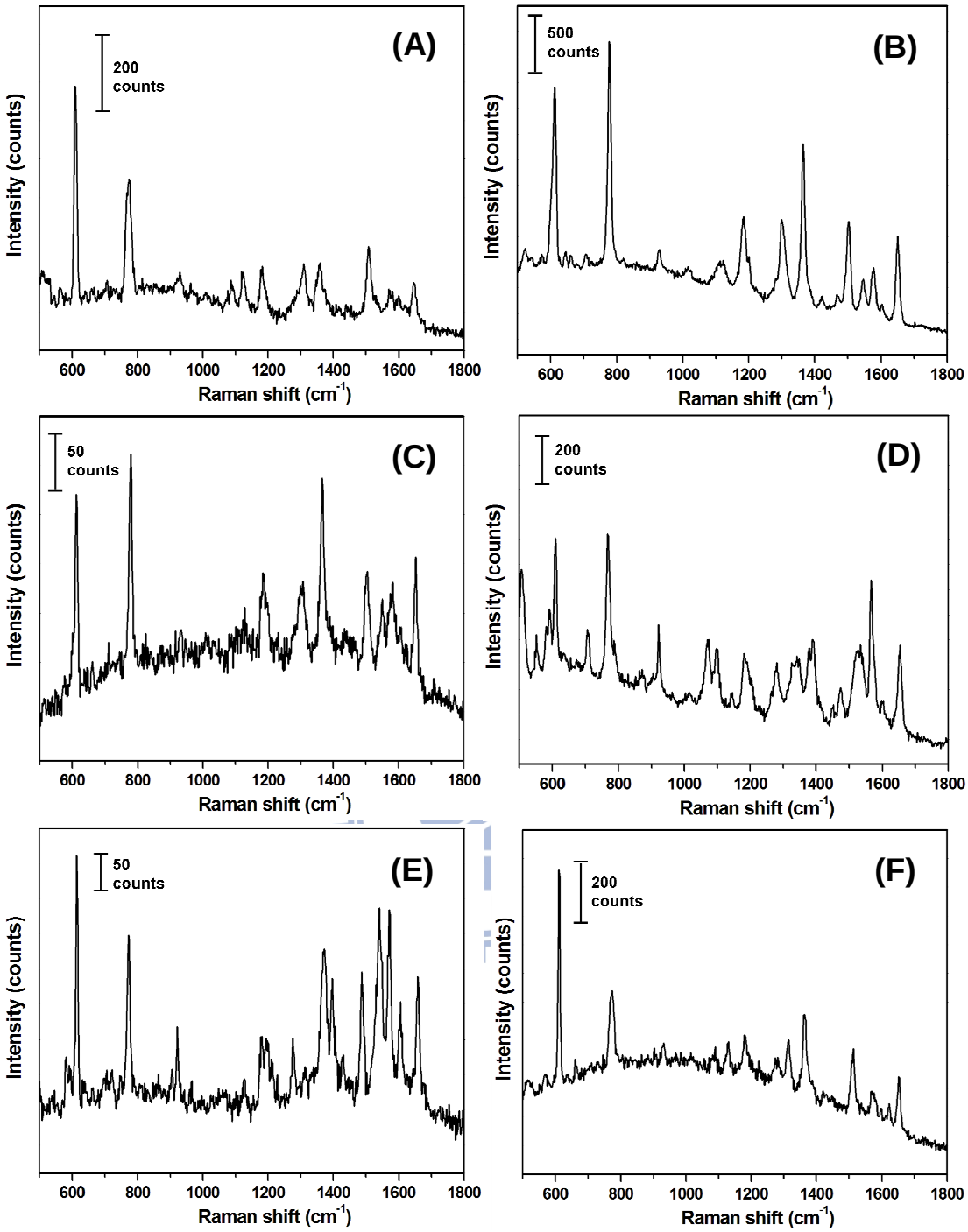

Figure 3.6 Raman spectra of the R6G signals in Figure 3.5. (A) (B) (C) spectra are the signals in Figure 3.5(B) from left to right. (D), (E), (F) spectra are the signals come from Figure3.5 (C), (E), (F), respectively.

are highly influenced by the local electrical field parallel or perpendicular to the molucles.[58,59] Another possible reason is that when molecules are trapped in the hot

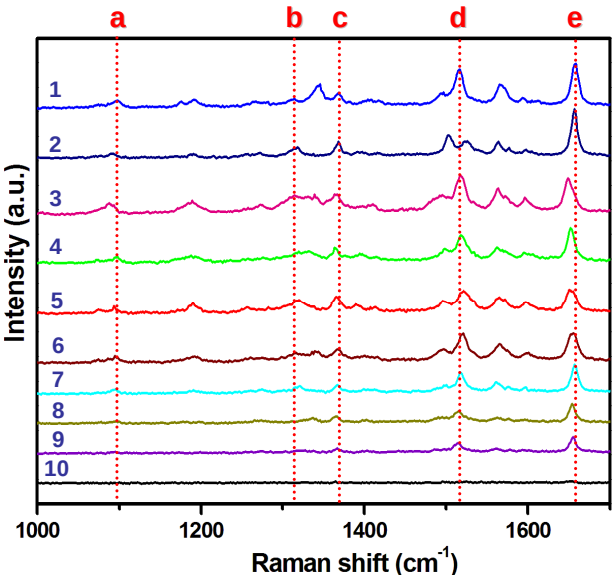

Spectrum	SERS signals (cm^{-1})				
	a	b	c	d	e
1	1098	1314	1368	1516	1658
2	1089	1318	1368	1526	1656
3	1088	1314	1366	1518	1648
4	1096	1319	1363	1518	1651
5	1092	1319	1365	1521	1650
6	1094	1316	1366	1521	1655
7	1096	1321	1366	1518	1656
8	x	x	1365	1515	1653
9	x	x	1366	1515	1655
10	x	x	x	x	x

Figure 3.7 Time-resolved surface-enhanced Raman spectra of R6G (10 μL, 1 fM) molecule recorded at 3-s intervals. Over 100 spectra were recorded before the signals disappeared. Ten spectra were selected to highlight sudden spectral changes. The table displayed five main Raman signals in these spectra. The Raman signals abruptly changed in both frequency and intensity. The laser excitation wavelength was 532 nm and the power was about 5 mW.

spots, some physical stress may be generated so that the adsorbed molecules undergo certain structural transformations[60] or photochemical decomposition.[25] In previous reports, most single molecule detections were carried out in special environment (i.e. on nanocrystal aggregates) or required multiple step modifications of sensing surfaces.[30-35] Our Ag NW substrate clearly shows the advantage of detecting a single molecule easily over the entire treated surface.

Intrinsic SERS enhancement factor (EF) is difficult to estimate because many variables, such as adsorbed molecules and laser scattering volume, are difficult to obtain.[61] Thus, we use the analytical enhancement factor (AEF), defined by the following equation: $AEF = (I_{SERS}/C_{SERS})/(I_{RS}/C_{RS})$,[61] to estimate the SERS performance of the urchin-like Ag NWs. Here, I_{RS} represents the Raman intensity of an analyte with

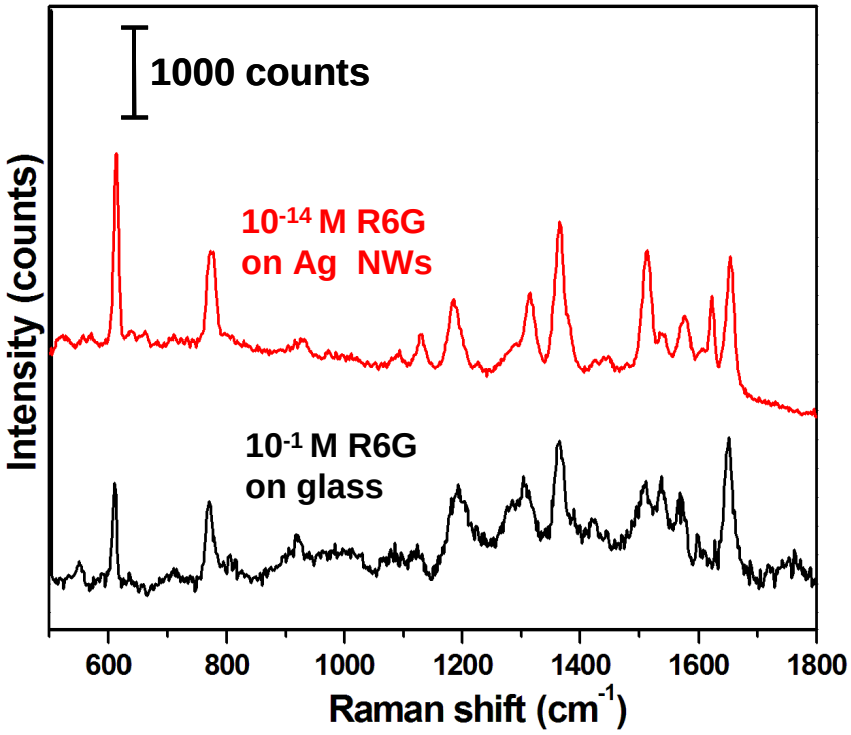

Figure 3.8 SERS of R6G on urchin-like Ag NWs (10 fM, red) and on a glass slide (0.1 M, black). (Excitation: 532 nm, power: 5 mW, data collection: 5 s).

a concentration C_{RS} on a non-SERS substrate. I_{SERS} is obtained from a SERS-active substrate with an analyte concentration C_{SERS}. In the studies, all the other parameters, including laser wavelength, laser power, microscope magnification, and spectrometer, are identical. In our experiment, a glass plate was used as the non-SERS substrate while the urchin-like Ag NWs was employed as the SERS-active one. The Raman responses of R6G on these substrates are compared in Figure 3.8. Using I_{RS} and I_{SERS} of the peaks at 614 cm^{-1}, 776 cm^{-1}, 1366 cm^{-1}, 1509 cm^{-1}, and 1650 cm^{-1} of R6G, the averaged *AEF* of the urchin-like Ag NWs substrate is estimated to be about 10^{13}. The value is superiior to most of the literature data listed in Table 3.2. In addition, on a commercial SERS-active substrate Klarite^{TM}, the signals from R6G (1 nM) almost vanished.[40] At higher R6G concentration such as 1 pM, fifteen randomly selected spots on urchin-like Ag NWs substrate ususally displayed similar SERS performance.

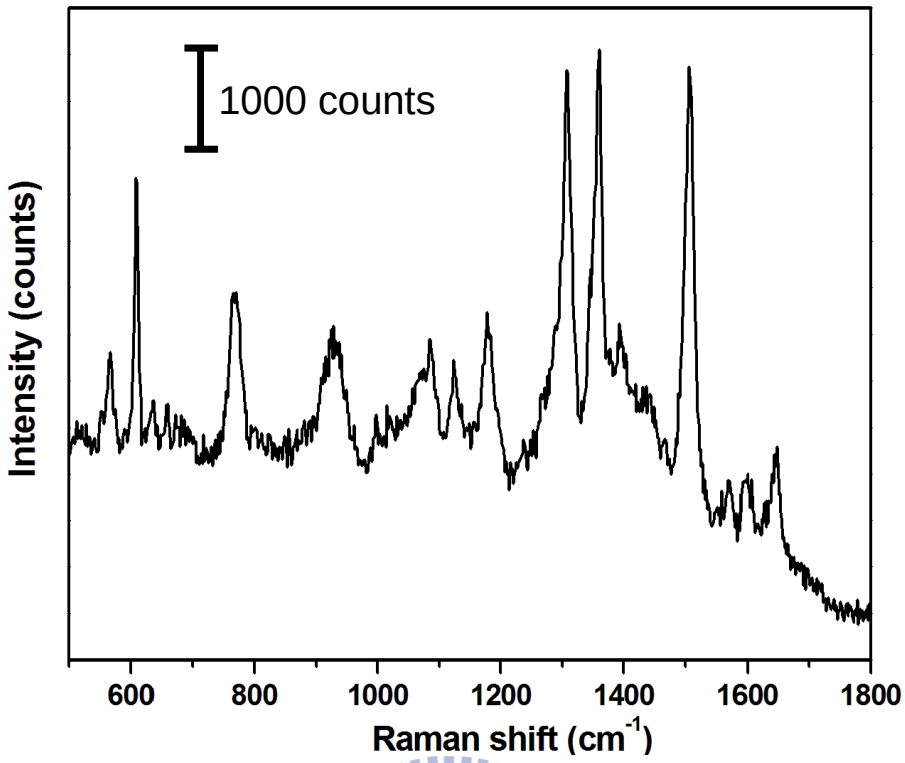

Figure 3.9 Raman spectrum of R6G (1 μM, 10 μL, in ethanol) on urchin-like silver NWs (Detected by MiniRam™ II Raman Spectrometer System, excitation: 785 nm, power: 5 mW, data collection: 5 s).

Different urchin-like Ag NWs substrates showed similar results. We also employed a low-cost portable Raman instrument with an excitation wavelength 785 nm to study potential SERS application of our Ag NWs. As shown in Figure 3.9, the R6G (1 μM, 10 μL in ethanol) signals were observed clearly. The result suggests that by coupling our Ag NW substrate with a low-cost portable apparatus, it is possible to find economical and real-life sensing applications.[62-65]

3.4 Conclusion

In this study, we have developed a simple low-cost surfactant-assisted galvanic reduction process to grow urchin-like Ag NWs on carbon screen printed electrodes. The urchin-like Ag NW substrate shows a high SERS performance. Using R6G as the probe molecule, the test needs only a minute quantity of sample solution (10 μL) with a short sensing time (5 s). The AEF is high (10^{13}). The detection limit for R6G is below femto molar concentration. This means the sensing is at single molecular level for R6G. Consequently, we anticipate that by coupling the urchin-like Ag NWs with a low-cost portable instrument, the setup can be applied for rapid biological, medicine, and environmental pollutant sensing applications. The investigation is in progress.

3.5 References

1. Fleischmann, M.; Hendra, P. J.; McQuillan, A. J. *Chem. Phys. Lett.* **1974,** *26*, 163.
2. Albrecht, M. G.; Creighton, J. A. *J. Am. Chem. Soc.* **1977,** *99*, 5215.
3. Jeanmaire, D. L.; Van Duyne, R. P. *J. Electroanal. Chem.* **1977,** *84*, 1.
4. Wang, H. H.; Liu, C. Y.; Wu, S. B.; Liu, N. W.; Peng, C. Y.; Chan, T. H.; Hsu, C. F.; Wang, J. K.; Wang, Y. L. *Adv. Mater.* **2006,** *18*, 491.
5. Lee, S. J.; Morrill, A. R.; Moskovits, M. *J. Am. Chem. Soc.* **2006,** *128*, 2200.
6. Tao, A.; Kim, F.; Hess, C.; Goldberger, J.; He, R.; Sun, Y.; Xia, Y.; Yang, P. *Nano Lett.* **2003,** *3*, 1229.
7. Liu, Y. J.; Chu, H. Y.; Zhao, Y. P. *J. Phys. Chem. C* **2010,** *114*, 8176.
8. Sun, Y.; Wiederrecht, G. P. *Small* **2007,** *3*, 1964.
9. Lin, H.; Mock, J.; Smith, D.; Gao, T.; Sailor, M. J. *J. Phys. Chem. B* **2004,** *108*, 11654.
10. Wen, X.; Xie, Y.-T.; Mak, W. C.; Cheung, K. Y.; Li, X.-Y.; Renneberg, R.; Yang, S. *Langmuir* **2006,** *22*, 4836.
11. Song, W.; Cheng, Y.; Jia, H.; Xu, W.; Zhao, B. *J. Colloid Interface Sci.* **2006,** *298*, 765.
12. Gutés, A.; Carraro, C.; Maboudian, R. *J. Am. Chem. Soc.* **2010,** *132*, 1476.
13. Rashid, H.; Mandal, T. K. *J. Phys. Chem. C* **2007,** *111*, 16750.
14. Hong, B. H.; Bae, S. C.; Lee, C. W.; Jeong, S.; Kim, K. S. *Science* **2001,** *294*, 348.
15. Jin, R.; Cao, Y.; Mirkin, C. A.; Kelly, K. L.; Schatz, G. C.; Zheng, J. G. *Science* **2001,** *294*, 1901.
16. Jana, N. R.; Gearheart, L.; Murphy, C. J. *Chem. Commun.* **2001**, 617.
17. Sun, Y.; Xia, Y. *Adv. Mater.* **2002,** *14*, 833.

18. Choi, J.; Sauer, G.; Nielsch, K.; Wehrspohn, R. B.; Gösele, U. *Chem. Mater.* **2003,** *15*, 776.

19. Sun, Y. *Chem. Mater.* **2007,** *19*, 5845.

20. Qin, L. D.; Zou, S. L.; Xue, C.; Atkinson, A.; Schatz, G. C.; Mirkin, C. A. *Proc. Natl. Acad. Sci. U. S. A.* **2006,** *103*, 13300.

21. Wang, Z. B.; Luk'yanchuk, B. S.; Guo, W.; Edwardson, S. P.; Whitehead, D. J.; Li, L.; Liu, Z.; Watkins, K. G. *J. Chem. Phys.* **2008,** *128*, 094705.

22. Chen, C.; Hutchison, J. A.; Clemente, F.; Kox, R.; Uji-I, H.; Hofkens, J.; Lagae, L.; Maes, G.; Borghs, G.; Van Dorpe, P. *Angew. Chem. Int. Ed.* **2009,** *48*, 9932.

23. Prokes, S. M.; Glembocki, O. J.; Rendell, R. W.; Ancona, M. G. *Appl. Phys. Lett.* **2007,** *90*, 093105.

24. Prokes, S. M.; Alexson, D.; Glembocki, O. J.; Park, H. D.; Rendell, R. W. *J. Vac. Sci. Technol. B* **2009,** *27*, 2055.

25. Nie, S.; Emory, S. R., *Science* **1997,** *275*, 1102.

26. Kneipp, K.; Wang, Y.; Kneipp, H.; Perelman, L. T.; Itzkan, I.; Dasari, R. R.; Feld, M. S. *Phys. Rev. Lett.* **1997,** *78*, 1667.

27. Wilson, R.; Bowden, S. A.; Parnell, J.; Cooper, J. M. *Anal. Chem.* **2010,** *82*, 2119.

28. Rao, S.; Raj, S.; Balint, S.; Fons, C. B.; Campoy, S.; Llagostera, M.; Petrov, D. *Appl. Phys. Lett.* **2010,** *96*, 213701.

29. Wang, Y.; Lee, K.; Irudayaraj, J. *J. Phys. Chem. C* **2010,** *114*, 16122.

30. Michaels, A. M.; Jiang; Brus, L. *J. Phys. Chem. B* **2000,** *104*, 11965.

31. Bosnick, K. A.; Jiang, J.; Brus, L. E. *J. Phys. Chem. B* **2002,** *106*, 8096.

32. Futamata, M.; Maruyama, Y.; Ishikawa, M. *Vib. Spectrosc* **2004,** *35*, 121.

33. Futamata, M.; Maruyama, Y.; Ishikawa, M. *J. Phys. Chem. B* **2004,** *108*, 13119.

34. Sawai, Y.; Takimoto, B.; Nabika, H.; Ajito, K.; Murakoshi, K. *J. Am. Chem. Soc.*

2007, *129*, 1658.

35. Lim, D.-K.; Jeon, K.-S.; Kim, H. M.; Nam, J.-M.; Suh, Y. D. *Nat. Mater.* **2010,** *9*, 60.
36. Hsia, C.-H.; Yen, M.-Y.; Lin, C.-C.; Chiu, H.-T.; Lee, C.-Y. *J. Am. Chem. Soc.* **2003,** *125*, 9940.
37. Wang, L. S.; Buchholz, D. B.; Li, Y.; Li, J.; Lee, C. Y.; Chiu, H. T.; Chang, R. P. H. *Appl. Phys. A* **2007,** *87*, 1.
38. Huang, T.-K.; Cheng, T.-H.; Yen, M.-Y.; Hsiao, W.-H.; Wang, L.-S.; Chen, F.-R.; Kai, J.-J.; Lee, C.-Y.; Chiu, H.-T. *Langmuir* **2007,** *23*, 5722.
39. Huang, T.-K.; Chen, Y.-C.; Ko, H.-C.; Huang, H.-W.; Wang, C.-H.; Lin, H.-K.; Chen, F.-R.; Kai, J.-J.; Lee, C.-Y.; Chiu, H.-T. *Langmuir* **2008,** *24*, 5647.
40. Yang, Y.-C.; Huang, T.-K.; Chen, Y.-L.; Mevellec, J.-Y.; Lefrant, S.; Lee, C.-Y.; Chiu, H.-T. *J. Phys. Chem. C* **2011,** *115*, 1932.
41. Sun, Y.; Gates, B.; Mayers, B.; Xia, Y. *Nano Lett.* **2002,** *2*, 165.
42. Moskovits, M. *Rev. Mod. Phys.* **1985,** *57*, 783.
43. Haynes, C. L.; Van Duyne, R. P. *J. Phys. Chem. B* **2003,** *107*, 7426.
44. Alvarez-Puebla, R.; Cui, B.; Bravo-Vasquez, J.-P.; Veres, T.; Fenniri, H. *J. Phys. Chem. C* **2007,** *111*, 6720.
45. Jackson, J. B.; Halas, N. J. *Proc. Natl. Acad. Sci. U. S. A.* **2004,** *101*, 17930.
46. Shim, S.; Stuart, C. M.; Mathies, R. A. *ChemPhysChem* **2008,** *9*, 697.
47. Hildebrandt, P.; Stockburger, M. *J. Phys. Chem.* **1984,** *88*, 5935.
48. Jensen, L.; Schatz, G. C. *J. Phys. Chem. A* **2006,** *110*, 5973.
49. Qiu, T.; Wu, X. L.; Shen, J. C.; Chu, P. K. *Appl. Phys. Lett.* **2006,** *89*, 131914.
50. Chen, H.; Wang, Y.; Qu, J.; Dong, S. *J. Raman Spectrosc.* **2007,** *38*, 1444.
51. Sakano, T.; Tanaka, Y.; Nishimura, R.; Nedyalkov, N. N.; Atanasov, P. A.; Saiki, T.; Obara, M. *J. Phys. D: Appl. Phys.* **2008,** *41*, 235304.

52. Duan, G. T.; Cai, W. P.; Luo, Y. Y.; Li, Z. G.; Li, Y. *Appl. Phys. Lett.* **2006,** *89*, 211905.

53. Zhou, Q.; Li, Z.; Yang, Y.; Zhang, Z. *J. Phys. D: Appl. Phys.* **2008,** *41*, 152007.

54. Galopin, E.; Barbillat, J.; Coffinier, Y.; Szunerits, S.; Patriarche, G.; Boukherroub, R. *ACS Appl. Mater. Interfaces* **2009,** *1*, 1396.

55. Liu, Y.-C.; Yu, C.-C.; Sheu, S.-F. *J. Mater. Chem.* **2006,** *16*, 3546.

56. Gutes, A.; Carraro, C.; Maboudian, R. *ACS Appl. Mater. Interfaces* **2009,** *1*, 2551.

57. Liu, Y.-C.; Yu, C.-C.; Hsu, T.-C. *Electrochem. Commun.* **2007,** *9*, 639.

58. Cai, W.-B.; Wan, L.-J.; Noda, H.; Hibino, Y.; Ataka, K.; Osawa, M. *Langmuir* **1998**, *14*, 6992.

59. Ru, E. C. L.; Meyer, M.; Blackie, E.; Etchegoin, P. G. *J. Raman Spectrosc.* **2008**, *39*, 1127.

60. Chen, T.; Wang, H.; Chen, G.; Wang, Y.; Feng, Y.; Teo, W. S.; Wu, T.; Chen, H. *ACS Nano* **2010**, *4*, 3087.

61. Le Ru, E. C.; Blackie, E.; Meyer, M.; Etchegoin, P. G. *J. Phys. Chem. C* **2007,** *111*, 13794.

62. Gao, L.; Fan, L.; Zhang, J. *Langmuir* **2009,** *25*, 11844.

63. Sun, X.; Lin, L.; Li, Z.; Zhang, Z.; Feng, J. *Mater. Lett.* **2009,** *63*, 2306.

64. Chen, H.; Simon, F.; Eychmüller, A. *J. Phys. Chem. C* **2010,** *114*, 4495.

65. Lv, S.; Suo, H.; Zhao, X.; Wang, C.; Jing, S.; Zhou, T.; Xu, Y.; Zhao, C. *Solid State Commun.* **2009,** *149*, 1755.

Chapter 4

Urchin-like Ag Nanowires as a Non-enzymatic Hydrogen Peroxide Sensor

4.1 Introduction

H_2O_2 is not only widely used in paper, cleaning product, and food industries,[1] but also generated as a by-product in several enzyme-catalyzed reactions.[2-5] A lot of analytic techniques have been developed to detect minute quantities of H_2O_2 such as titrimetry,[6] spectrophotometry,[7,8] chemiluminescence,[9-11] and electrochemistry.[12-14] Among them, electrochemical analysis has been considered as a low-cost and effective method due to its simplicity and high sensitivity. Until now, a great deal of H_2O_2 sensors have been developed based on electocatalysis of H_2O_2 reduction by immobilized enzymes.[15-17] However, these electrodes showed many disadvantages related to their stability and activity degradations of immobilized enzymes.[18,19] Therefore, there are more and more attempts to develop non-enzymatic sensors constructed from nanostructured materials. For example, in recent years, electrodes modified with metal nanoparticles (NPs) such as Pt NPs,[20,21] Au NPs,[22] Pd NPs[23] and Ag NPs,[24] have been extensively used for non-enzymatic H_2O_2 sensors. They usually showed large specific surface areas, excellent conductivities, and outstanding electrocatalytic activities. Because Ag is a relatively inexpensive noble metal of all, several kinds of Ag nanostructures have been fabricated for non-enzymatic H_2O_2 sensing applications.[25-27] Previously, we have reported the non-enzymatic glucose sensors such as Cu nanobelt[28] and Au nanocoral[29] on screen-printed carbon (SPC) electrodes via several heterogeneous reactions. We discovered that surfactant-assisted

galvanic reductions provide low cost, one step, and near room temperature growth routes. By using this strategy, recently, we demonstrated the growth of urchin-like Ag NWs on screen-printed carbon (SPC) electrodes.[30] Using the new electrode, we wish to report the first case of using Ag NWs for non-enzymatic H_2O_2 sensing. Our discoveries are discussed below.

4.2 Experimantal

4.2.1 Reagents

Silver nitrate (Mallinckrodt), cetyltrimethylammonium chloride (CTAC, Taiwan Surfactant), hydrogen chloride (TEDIA), nitric acid (Showa), sodium phosphate dibasic dihydrate (Aldrich), sodium phosphate monobasic monohydrate (JT-Baker), D-(+)-glucose (Aldrich), L-ascorbic acid (AA, Aldrich), uric acid (UA, Aldrich), sodium chloride (Aldrich), sodium bicarbonate (Aldrich), and hydrogen peroxide (Aldrich) were used without further purification.

4.2.2 Preparation of Urchin-like Ag NWs

Urchin-like Ag NWs were synthesized on an SPC electrode with a Cu foil and stored in a N_2 filled glove box to prevent excessive surface oxidation. More detail procedures were represented in chapter 2.2.

4.2.3 Preparation of Ag Microparticles

A glass vial containing $AgNO_3$ electrolyte (10 mL, 10 mM) was placed in a water bath controlled at 303 K. A two-electrode electrochemical cell composed of a DC power supply and two carbon electrodes (Figure 4.1). Ag microparticles were grown on the cathode, which was an SPC electrode purchased from Zensor R&D with a geometric area of 0.196 cm^2. The anode was fabricated by painting carbon paste uniformly on a transparent projection slide followed by drying it on a hotplate at 353 K for 3 h under air. After the cathode and the anode were immersed in the electrolyte

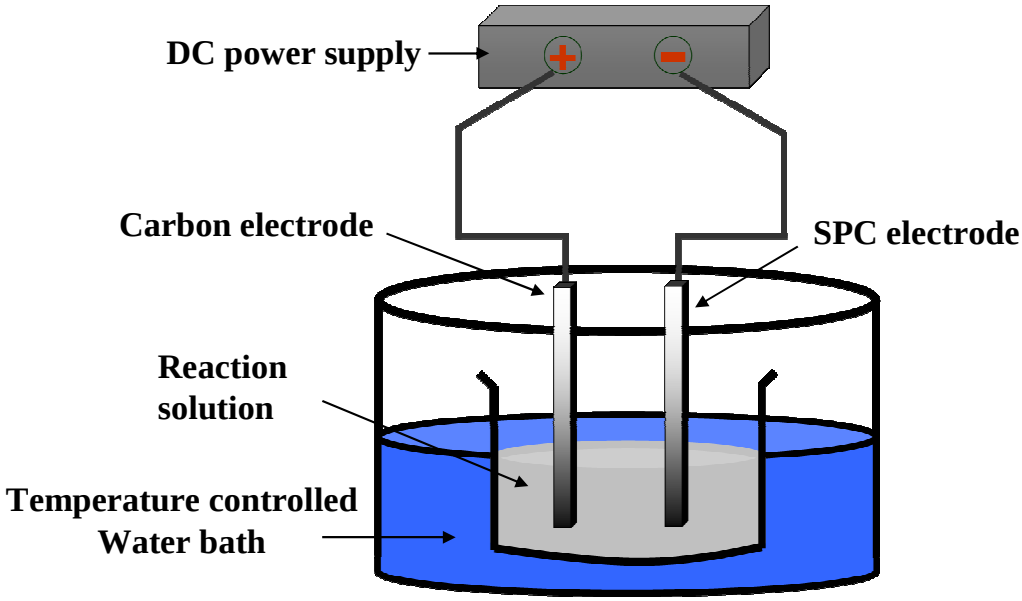

Figure 4.1 Two-electrode electrodeposition system.

for 2 min, a fixed DC voltage of 1.0 V was supplied across the electrodes. At 303 K without stirring, the cathode surface turned into gray color gradually. After 1 h, a total charge of ca. 0.24 C (corresponding to Ag 0.268 μg) was supplied. The cathode was removed and rinsed with deionized water. To avoid oxidation, the as-prepared Ag microparticles were stored in a N_2 filled glove box to prevent excessive surface oxidation.

4.2.4 Characterizations and Electrochemical Measurements

The scanning electron microscopic (SEM) and energy dispersive spectroscopic (EDS) data were taken from a Hitachi S-4000 (25 keV) and a JEOL JSM-7401F (15 keV). Cyclic voltammetric (CV) and amperometric experiments were carried out on a CHI 6081C (CH Instruments) electrochemical analyzer. A three electrode system was employed for the measurements. It contained a working electrode, which is a Ag electrode fabricated in this study, a counter electrode composed of a Pt wire, and an Ag/AgCl (in KCl 3.00M) reference electrode, with a potential of 0.200 V vs. standard hydrogen electrodes (SHE). Amperometric curves of hydrogen peroxide were

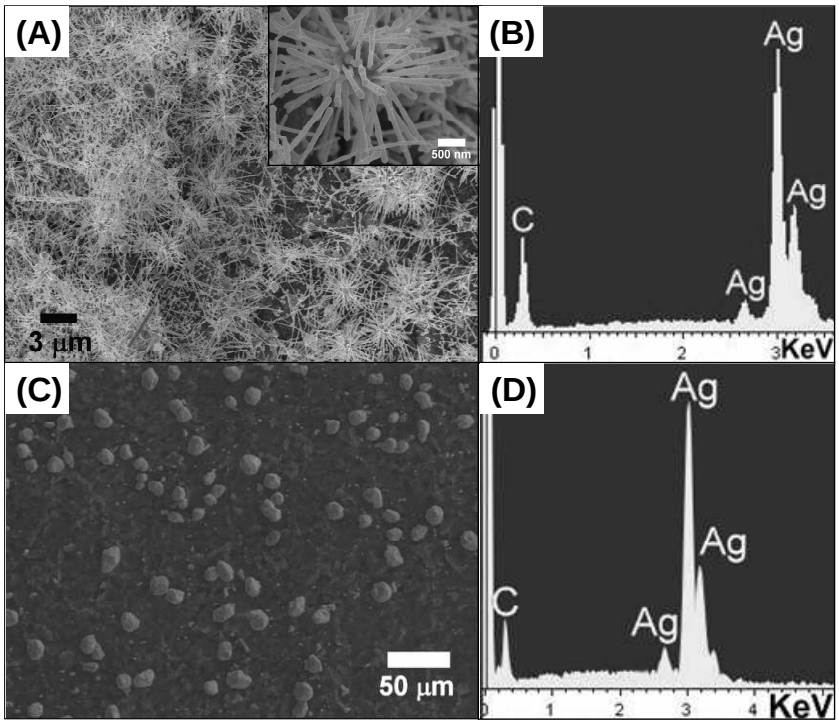

Figure 4.2 (A) SEM image of Ag urchin-like NWs on an SPC electrode (inset: enlarged view of a single cluster of urchin-like Ag NWs). (B) EDS of an area in part A. (C) SEM image of Ag microparticles on an SPC electrode. (D) EDS of an area in part C.

recorded at -0.28 V and -0.4 V for Ag NW and Ag microparticle electrodes, respectively. Before carrying out the electrochemical experiments, all of the solution were de-oxygenated by $N_{2(g)}$. Various amounts of hydrogen peroxide were added every 100 s into a stirring 0.01 M PBS (pH 7.4) solution in air.

4.3 Results and Discussion

4.3.1 SEM and EDS Characterizations

Figure 4.2 shows the SEM data of the as-prepared Ag NWs and Ag micro-particles. As displayed in Figure 4.2A, lots of Ag urchin-like NWs grow on the electrode surface. Based on the EDS (Figure 1B), we conclude that the NWs are composed of Ag only. The inset in Figure 4.2A shows an enlarged view of the urchin-like morphology. The diameters of the NWs are estimated to be about 100 nm

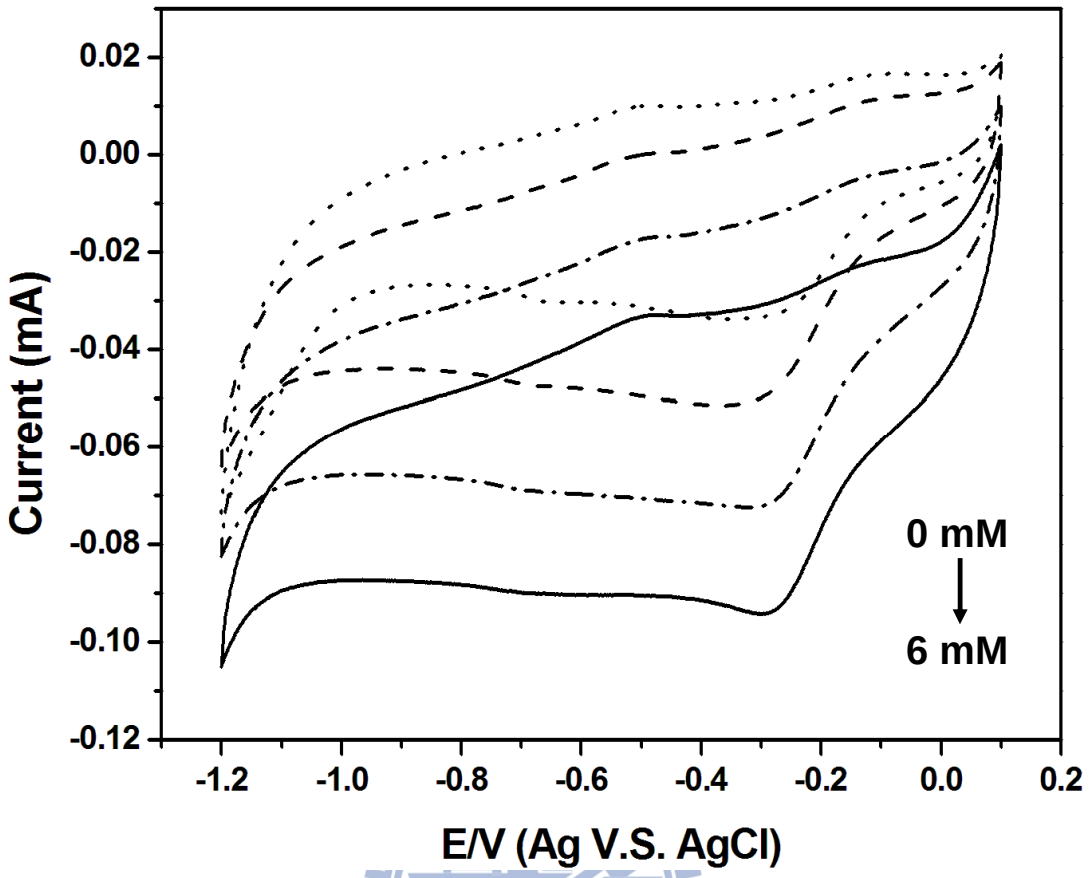

Figure 4.3 CVs of different H_2O_2 concentrations in deaerated PBS (pH 7.4, 0.01 M) using an Ag NW electrode as the working electrode. The H_2O_2 concentrations are 0 mM (dot), 2 mM (dash), 4 mM (dash dot), and 6 mM (solid). The scan rate is 50 mV/s.

while the lengths are found to be in the range 3 – 10 μm. Figure 4.2C displays the image of the microparticles. They are about 20 μm in diameters and composed of Ag (Figure 4.2D).

4.3.2 Cyclic Voltammetric Studies

Figure 4.3 shows the CV responses of different H_2O_2 concentrations on an Ag NW electrode. It indicats that the reduction current (at -0.28 V) gradually increases with the increasing of H_2O_2 concentration. Figure 4.4 displays the CVs in the absence (solid line) and presence (dashed line) of H_2O_2 (6 mM) in deaerated PBS (pH 7.4,

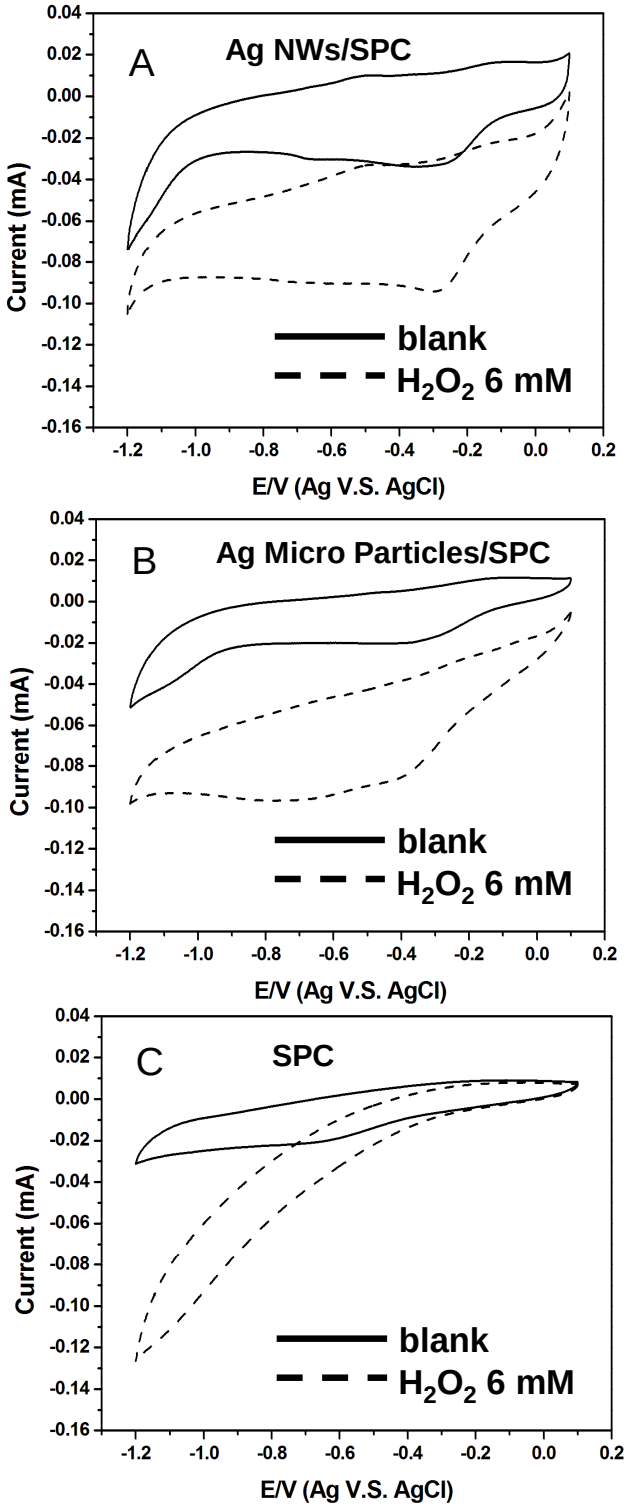

Figure 4.4 Comparison of CV scans before (solid) and after (dashed) addition of H_2O_2 (6 mM) in deaerated PBS (pH 7.4, 0.01 M). The working electrodes are (A) Ag NWs, (B) Ag microparticles and (C) screen printed carbon electrodes. The scan rate is 50 mV/s.

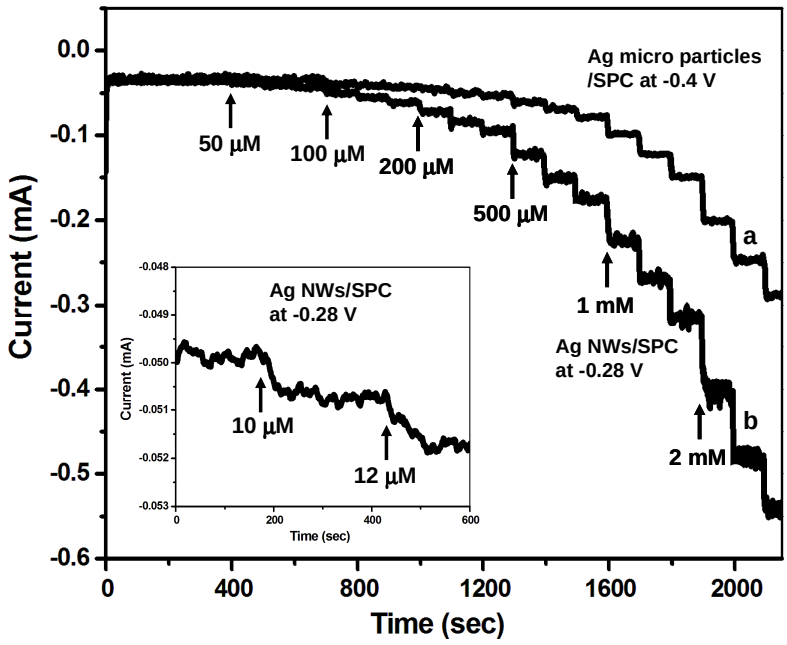

Figure 4.5 Amperometric current responses to successive additions of H_2O_2 in deaerated PBS (pH 7.4, 0.01 M) on (a) Ag micro particles electrode (black) at -0.4 V and (b) Ag NW electrode (red) at -0.28 V. Inset shows the lowest concentration to be detected at 10 µM.

0.01 M) using Ag NW, Ag microparticle, and SPC electrodes. We notice that the reduction current response from using the Ag NW is slightly larger than using the Ag microparticle electrode. Furthermore, the reduction potential of using the Ag NW electrode (-0.28 V) is also smaller than the value of using Ag micro particle electrode (-0.4 V). These results indicate that the Ag NW electrode possesses a relatively notable catalytic ability towards H_2O_2 reduction. It is known that the electrocatalytic properties of Ag nanoparticles depend on their dimension, density and amount deposited on electrode surfaces.[31,32] Since the Ag NWs on a SPC electrode had smaller size and higher density than the Ag microparticles on the electrode did, the reduction potential of using the Ag NW electrode displayed better electrocatalytic property and lower reduction potential for H_2O_2 reduction than the other electrode showed.

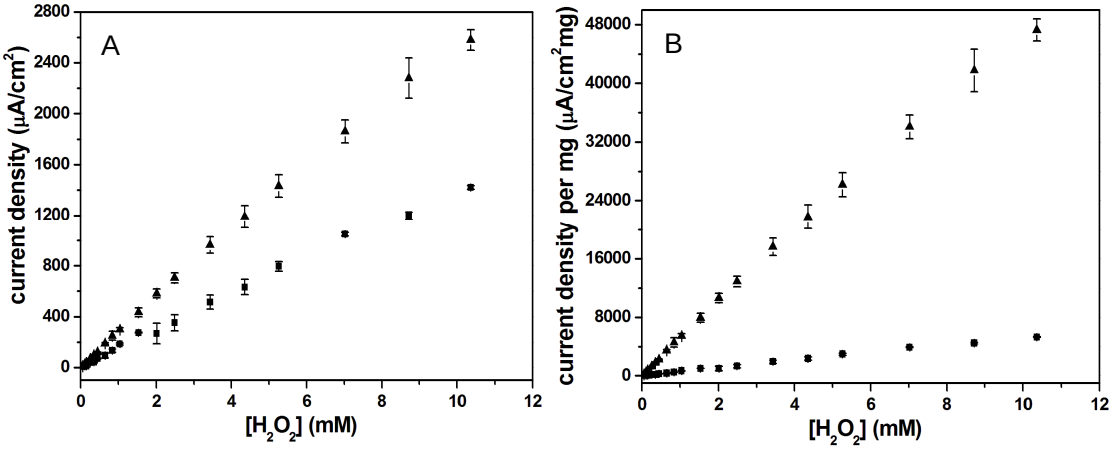

Figure 4.6 (A) Calibration curves of amperometric tests in Figure 5. (B) Calibration curves (current density normalized by mass) of amperometric tests in Figure 5. The working electrodes are Ag NWs (black triangle) and Ag microparticles (black square). The error bars indicated the standard deviation of three successive measurements.

4.3.3 Amperometric Studies of Hydrogen Peroxide Sensing

Figure 4.5 illustrates amperometric measurements of H_2O_2 in PBS (0.01 M) using the Ag NW electrode (-0.28 V) and Ag microparticle electrode (-0.4 V). The former electrode provides higher reduction current response than the second one does. The inset in Figure 4.5 shows that the detection limit of H_2O_2 is 10 μM. A sensitivity of 257 μA mM^{-1} cm^{-2} with a linear dependence (R^2 value, 0.998) of the reduction current to the H_2O_2 concentration (50 μM - 10.35 mM) is observed for the Ag NW electrode, which is slightly higher than the data observed for Ag microparticle electrode (138 μA cm^{-2} mM^{-1}). The calibration curves are derived from the amperometric tests in Figure 4.5 and showed in Figure 4.6A. When we take the Ag masses into account, normalized calibration curves of the amperometric measurements are obtained and shown in Figure 4.6B. The mass of Ag NWs is determined by using stripping voltammetry[33] (Figure 4.7). It can be seen clearly that the sensitivity of the Ag NW electrode (4705 μA mM^{-1} mg^{-1} cm^{-2}) is much superior to

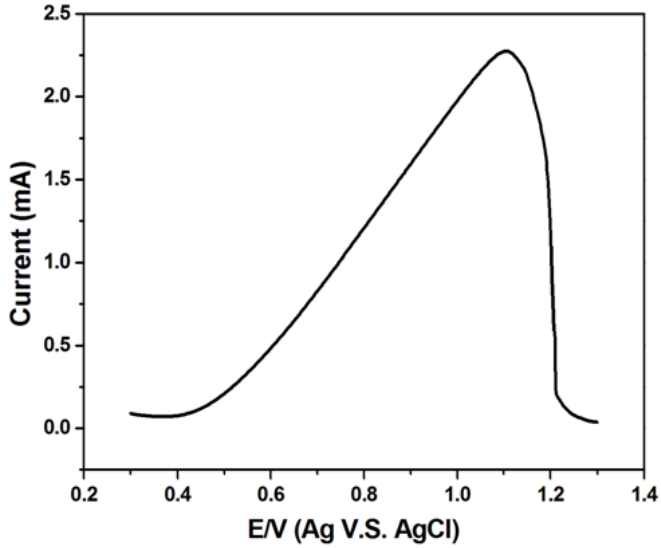

Figure 4.7 Stripping voltammetry of Ag NWs in a 0.1 M $NaClO_4$ solution at a scan rate ν = 20 mV/s.

the Ag microparticle one (540 μA mM^{-1} mg^{-1} cm^{-2}). Based on this evidence, we conclude that the Ag NWs have batter electrocatalytic property than the Ag microparticles do. Performances of various nanostructured non-enzymatic Ag electrodes reported previously are summarized in Table 4.1.[22-27,32,34-40] In general, our NW electrode performed equally or better than the reported cases did. Although the amount of Ag micro-spheres (25.6 μg) on glass carbon (GC) electrode[25] is less than the Ag NWs (54.6 μg) we made, the linear range of our electrode (0.05-10.35 mM) is much higher than the other one (0.25-2 mM). The applied potential of our Ag NW electrode is also lower than the Ag micro-sphere electrode (-0.5 V). For other electrodes, most of them did not show the amount of Ag on the electrodes. This makes quantitative comparisons difficult. The electrode with equal amount of Ag deposited showed similar performance for H_2O_2. We anticipate that the performance of our NW electrode could be enhanced further by adjusting the amount of Ag deposited and the geometric area employed. Other noble metal based non-enzymatic

H_2O_2 sensors such as Au[22] and Pd[23] are usually expensive and require multiple synthetic steps. To our knowledge, our study is the first report on Ag NWs for non-enzymatic H_2O_2 sensor application.

Table 4.1 Comparison of various non-enzymatic H_2O_2 sensors

electrode	Applied potential	Mass (μg)	Sensitivity ($\mu A\ mM^{-1}cm^{-2}$)	Linear range (mM)	Detection limit (μM)	Ref.
Ag NPs/type Ⅰ collagen/GC	-0.300 V[a]	-	-	0.005-40.6	0.7[b]	32
Ag-DNA hybrid NPs/GC	-0.45 V[a]	-	773	0.002-2.5	0.6[b]	24
Ag NPs/DNA network/GC	-0.400 V[a]	-	-	0.004-16	1.7[b]	34
MWNTs/Ag nanohybids on Au electrode	-0.2 V[c]	-	1.42[d]	0.05-17	0.5[b]	35
Ag micro-spheres/GC	-0.5 V[a]	25.6	-	0.25-2	1.2[b]	25
Roughened Ag	-0.30 V[a]	-	-	0.01-22.5	6[b]	36
Ag NPs-NFs/GC	-0.30 V[c]	-	-	0.1-80	62[b]	37
Ag nano-sieve/GC	-0.44 V[c]	-	-	0.04-900[e]	10[b]	27
AgNP-decorated PMPD micro-particle/GC	-0.300 V[c]	-	-	0.1-30	4.7[b]	38
AgNPs/ZnO NRs/FTO	-0.55 V[c]	-	152.1	0.008–0.983	0.9[b]	39
AgNPs/PVA/Pt	-0.500 V[a]	-	4090	0.04-6	1[b]	40
Ag dendrite/GC	-0.2 V[c]	-	104.53	0.005-12	0.5[b]	26
Pd/CNF-CPE	-0.2 V[c]	-	4.15[f]	0.2-20	0.2[b]	23
Au NPs/OMC/GC	-0.15 V[c]	-	-	0.002-3.92	0.49[b]	22
Ag Urchin-like NWs/SPC	-0.28 V[c]	54.6	256.9	0.05-10.35	10[f]	This work
Ag micro particles/SPC	-0.40 V[c]	268	124.1	0.05-14.20	50[f]	This work

a: referred to a saturated calomel electrode (SCE) (0.242 V versus SHE)

b: theoratical detection limit (estimated from three times of the standard deviation of the blank signal)

c: referred to an Ag/AgCl (in KCl 3.00 M) electrode (0.200 V versus SHE)

d: the unit is $\mu A\ mM^{-1}$

e: acidic media

f: smallest addition

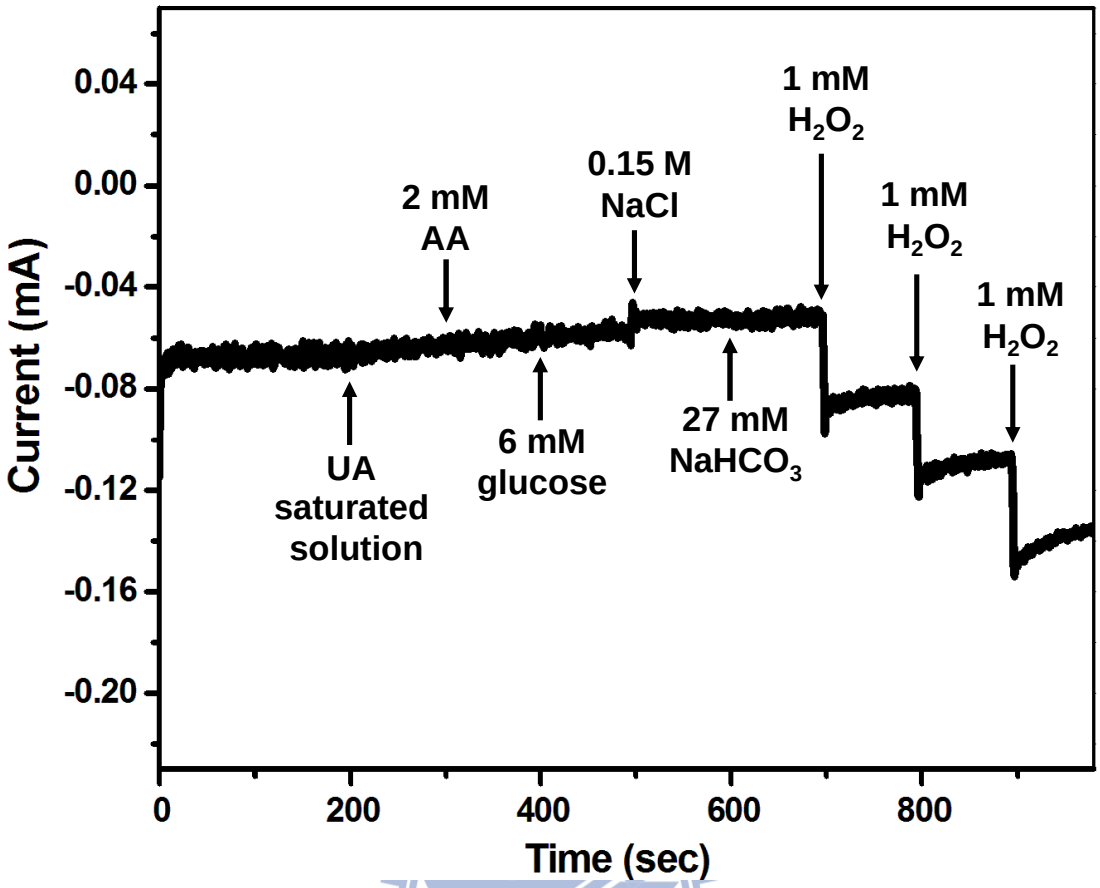

Figure 4.8 Interference analysis by amperometry at -0.28 V. The injection sequences are UA (saturated), AA (2 mM), glucose (6 mM), NaCl (0.15 M), $NaHCO_3$ (27 mM), followed by H_2O_2 (1 mM) additions in deaerated PBS (pH 7.4, 0.01 M).

4.3.4 Interference Studies

For interference test, we choose five common species L-ascorbic acid (AA), uric acid (UA), glucose, chloride ion (Cl^-), and hydrogen carbonate ion (HCO_3^-) found commonly in real physiological samples.[41] We used concentrations comparable to the ones reported for our experiments. Amperometric responses of the Ag NW electrode towards the additions of these species (AA: 2 mM, UA: staturated, glucose: 6 mM, Cl^-: 150 mM, HCO_3^-: 27 mM) followed by H_2O_2 (1 mM successively) were examined. As shown in Figure 4.8, AA, UA, and glucose do not produce significant responses. Moreover, the anions of Cl^- and HCO_3^- have no obvious interference in the reduction

of H_2O_2. The observations reveal the application potential of Ag NWs electrode for sensing H_2O_2 in real samples.

4.4 Conclusion

In conclusion, we have demonstrated a simple low-cost galvanic displacement process to grow urchin-like Ag NWs on SPC electrodes for H_2O_2 sensing. Our results indicate that the Ag NW electrode shows higher electrocatalytic ability of H_2O_2 reduction than the Ag microparticle electrode does. The Ag NW electrode shows that its sensitivity for H_2O_2 reduction at an applied potential -0.28 V in PBS is 4705 μA mM^{-1} mg^{-1} cm^{-2}. The detection limit is observed at 10 μM. This is the first report on using Ag NWs for non-enzymatic H_2O_2 sensing application. The electrode can detect H_2O_2 easily and resists many interfering species commonly found in real physiological samples.

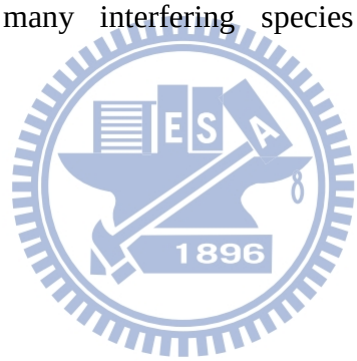

4.5 References

1. Prodromidis, M. I.; Karayannis, M. I. *Electroanalysis* **2002,** *14*, 241.
2. Guilbault G. G., Handbook of Enzymic Methods of Analysis, Dekker, New York, 1976.
3. Darder, M.; Takada, K.; Pariente, F.; Lorenzo, E.; Abruña, H. D. *Anal. Chem.* **1999,** *71*, 5530.
4. Masullo, M.; Raimo, G.; DelloRusso, A.; Bocchini, V.; Bannister, J. V. *Biotechnol. Appl. Biochem.* **1996,** *23*, 47.
5. Jiang, Y.; Miles, P. W. *Phytochemistry* **1993,** *33*, 29.
6. Brestovisky, A.; Kirowaeisner, E.; Osteryoung, J. *Anal. Chem.* **1983,** *55*, 2063.
7. Rinsland, C. P.; Coheur, P. F.; Herbin, H.; Clerbaux, C.; Boone, C.; Bernath, P.; Chiou, L. S. *J. Quant. Spectrosc. Radiat. Transf.* **2007,** *107*, 340.
8. Fernandes, K. F.; Lima, C. S.; Lopes, F. M.; Collins, C. H. *Process Biochem.* **2005,** *40*, 3441.
9. Yamashiro, N.; Uchida, S.; Satoh, Y.; Morishima, Y.; Yokoyama, H.; Satoh, T.; Sugama, J.; Yamada, R. *J. Nucl. Sci. Technol.* **2004,** *41*, 890.
10. Janasek, D.; Spohn, U. *Sens. Actuator B-Chem.* **1997,** *39*, 291.
11. Pehrman, R.; Amme, M.; Cachoir, C. *Czech. J. Phys.* **2006,** *56*, D373.
12. Shao, M. W.; Shan, Y. Y.; Wong, N. B.; Lee, S. T. *Adv. Funct. Mater.* **2005,** *15*, 1478.
13. Qiao, Y. B.; Yang, G.; Jian, F. F.; Qin, Y. Q.; Yang, L. R. *Sens. Actuator B-Chem.* **2009,** *141*, 205.
14. Shen, Y.; Trauble, M.; Wittstock, G. *Anal. Chem.* **2008,** *80*, 750.
15. Song, Y.; Wang, L.; Ren, C.; Zhu, G.; Li, Z. *Sens. Actuator B:Chem.* **2006,** *114*, 1001.
16. Guo, C.; Song, Y.; Wei, H.; Li, P.; Wang, L.; Sun, L.; Sun, Y.; Li, Z. *Anal.*

Bioanal. Chem. **2007,** *389*, 527.

17. Ferapontova, E.; Schmengler, K.; Börchers, T.; Ruzgas, T.; Gorton, L. *Biosens. Bioelectron.* **2002,** *17*, 953.
18. Willner, I.; Katz, E. *Angew. Chem. Int. Ed.* **2000,** *39*, 1180.
19. Xiao, Y.; Patolsky, F.; Katz, E.; Hainfeld, J. F.; Willner, I. *Science* **2003,** *299*, 1877.
20. Polsky, R.; Gill, R.; Kaganovsky, L.; Willner, I. *Anal. Chem.* **2006,** *78*, 2268.
21. Li, J. P.; Yu, Q. L.; Peng, T. Z. *Anal. Sci.* **2005,** *21*, 377.
22. Wang, L. X.; Bo, X. J.; Bai, J.; Zhu, L. D.; Guo, L. P. *Electroanalysis* **2010,** *22*, 2536.
23. Huang, J.; Wang, D.; Hou, H.; You, T. *Adv. Funct. Mater.* **2008,** *18*, 441.
24. Wu, S.; Zhao, H. T.; Ju, H. X.; Shi, C. G.; Zhao, J. W. *Electrochem. Commun.* **2006,** *8*, 1197.
25. Zhao, B.; Liu, Z. R.; Liu, Z. L.; Liu, G. X.; Li, Z.; Wang, J. X.; Dong, X. T. *Electrochem. Commun.* **2009,** *11*, 1707.
26. Qin, X.; Wang, H. C.; Wang, X. S.; Miao, Z. Y.; Fang, Y. X.; Chen, Q.; Shao, X. G. *Electrochim. Acta* **2011,** *56*, 3170.
27. Singh, R. P.; Pandey, A. C. *Anal. Methods* **2011,** *3*, 586.
28. Huang, T. K.; Lin, K. W.; Tung, S. P.; Cheng, T. M.; Chang, I. C.; Hsieh, Y. Z.; Lee, C. Y.; Chiu, H. T. *J. Electroanal. Chem.* **2009,** *636*, 123.
29. Cheng, T.-M.; Huang, T.-K.; Lin, H.-K.; Tung, S.-P.; Chen, Y.-L.; Lee, C.-Y.; Chiu, H.-T. *ACS Appl. Mater. Interfaces* **2010,** *2*, 2773.
30. Hsiao, W.-H.; Chen, H.-Y.; Yang, Y.-C.; Chen, Y.-L.; Lee, C.-Y.; Chiu, H.-T. *ACS Appl. Mater. Interfaces* **2011**, *3*, 3280.
31. Welch, C. M.; Banks, C. E.; Simm, A. O.; Compton, R. G. *Anal. Bioanal. Chem.* **2005,** *382*, 12.

32. Yonghai, S.; Kang, C.; Li, W.; Shouhui, C. *Nanotechnol.* **2009,** *20*, 105501 (8 pp.).

33. Jones, S. E. W.; Campbell, F. W.; Baron, R.; Xiao, L.; Compton, R. G. *J. Phys. Chem. C* **2008,** *112*, 17820.

34. Cui, K.; Song, Y. H.; Yao, Y.; Huang, Z. Z.; Wang, L. *Electrochem. Commun.* **2008,** *10*, 663.

35. Zhao, W.; Wang, H. C.; Qin, X.; Wang, X. S.; Zhao, Z. X.; Miao, Z. Y.; Chen, L. L.; Shan, M. M.; Fang, Y. X.; Chen, Q. *Talanta* **2009,** *80*, 1029.

36. Lian, W. P.; Wang, L.; Song, Y. H.; Yuan, H. Z.; Zhao, S. C.; Li, P.; Chen, L. L., *Electrochim. Acta* **2009,** *54*, 4334.

37. Tian, J. Q.; Liu, S.; Sun, X. P. *Langmuir* **2010,** *26*, 15112.

38. Tian, J. Q.; Li, H. L.; Lu, W. B.; Luo, Y. L.; Wang, L.; Sun, X. P. *Analyst* **2011,** *136*, 1806.

39. Lin, C. Y.; Lai, Y. H.; Balamurugan, A.; Vittal, R.; Lin, C. W.; Ho, K. C. *Talanta* **2010,** *82*, 340.

40. Guascito, M. R.; Filippo, E.; Malitesta, C.; Manno, D.; Serra, A.; Turco, A. *Biosensors & Bioelectronics* **2008,** *24*, 1057.

41. These concentrations of common species in blood can be found at the Web site: http://en.wikipedia.org/wiki/Reference_ranges_for_blood_tests

Chapter 5

Conclusions and Perspectives

5.1 Conclusions and Perspectives

In this study, we demonstrated the fabrication of urchin-like Ag NWs on a screen-printed-carbon electrode via galvanic reduction near room temperature. In this reaction, CTAC plays a role of capping reagent to confine and stabilize crystal growth to form the nanowires. On the other hand, NO_3^- may provide a selective etching ability on less stable facets during the crystal growth. Moreover, we reveal that Ag NWs are also synthesized successfully by using the same reaction solution via electrochemical deposition on ITO substrates with Au or Pt seeding layers. This may extend the fabrication of Ag NWs with Au or Pt seeding layers on other solid substrates by electrochemical deposition. We conclude that Ag NWs could be fabricated by either galvanic reduction or electrochemical deposition by surfactant assisted growth method.

Furthermore, we have explored the SERS property of the urchin-like Ag NWs. R6G was employed as a probe molecule. We discovered that the presence of 0.1 fM of R6G on the Ag NWs can be clearly observed, which is the lowest detection limit reported previously. SERS hot-spots of urchin-like Ag NWs may originate from short and sparse Ag NWs which would create few gaps, slits, and vacancies. The detection limit indicated that the sensing is at single molecule level. Single molecule detection was confirmed by the SERS mapping images. The AEF of the Ag NWs was estimated to be 10^{13}.

In addition, Ag NWs also display high electro-catalytic ability of H_2O_2 reduction.

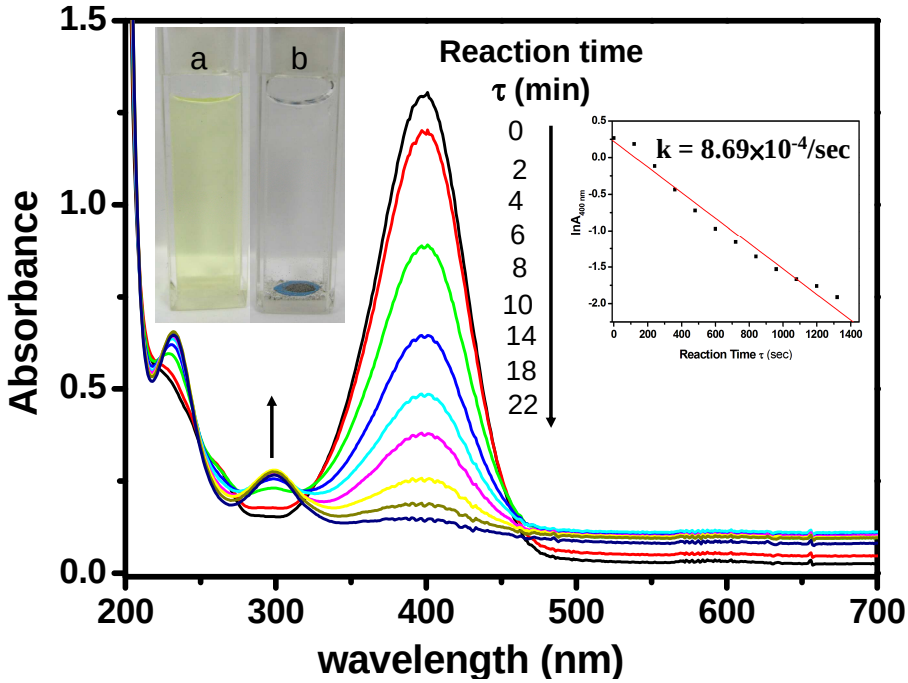

Figure 5.1 Successive UV-vis absorption spectra of the reduction of 4-NP by $NaBH_4$ in the presence of Ag NWs (t=22 min). The right inset shows the logarithm of the absorbance at 400 nm vs reduction time. The left inset shows the photographs of the reduction of 4-NP by $NaBH_4$ in the absence (a) and presence (b) of Ag NWs.

The sensitivity for H_2O_2 reduction at an applied potential -0.28 V in PBS is 4705 μA mM^{-1} mg^{-1} cm^{-2}. The detection limit is observed at 10 μM. This is the first report on using Ag NWs for non-enzymatic H_2O_2 sensing application.

More applications such as catalytic reduction of aromatic nitro compounds and antibacterial property are under investigations. Preliminary data are shown below. Catalytic reduction of aromatic nitro compounds by coinage metal nanoparticles has been reported.[1] Figure 5.1 shows the time evolution of UV spectra for the conversion of 4-nitrophenol (4-NP) into 4-aminophenol (4-AP). The absorption of 4-NP is at 400 nm and 4-AP is at 300 nm. We observe that the peak of 400 nm is getting lower and the one of 300 nm is getting stronger. The pseudo-first-order rate constant determined from this plot is 8.69×10^{-4} s^{-1}. Besides, the original color of the solution is slight

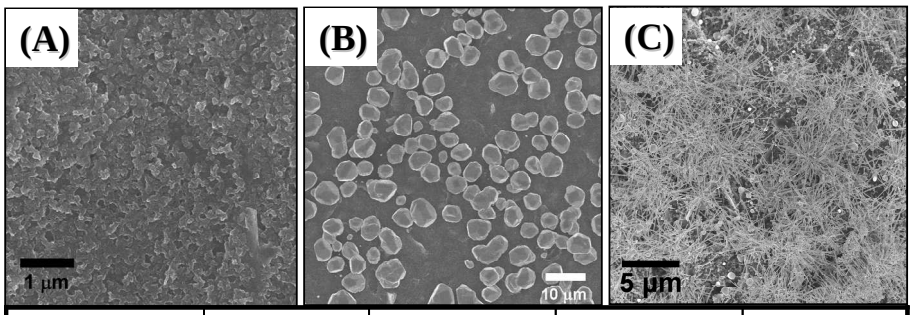

Sample	Blank	(A)	(B)	(C)
OD (600 nm)	0.4486	0.45705	0.47895	0.2327

Figure 5.2 Optical Density at 600 nm in tubes with different samples. (A) SPC electrode (B) Ag microparticles/SPC electrode (C) Ag NWs/SPC electrode.

yellow and become limpid after the reaction.

On the other hand, nanosilver has emerged as one of the most commercialized nanomaterials, particularly as antimicrobial agents with interesting applications such as wound dressings,[2] textiles,[3] and water and air purification.[4] A simple antibacterial test is shown below. We put different samples (screen printed carbon (SPC) electrode, Ag microparticles/SPC electrode, Ag NWs/SPC electrode) into tubes with Luria–Bertani (LB) medium and equal amount of Escherichia coli (E. coli) solution at 310 K. After 18 hours, the bacterial concentrations were determined by measuring optical density (OD) at 600 nm, which were displayed in Figure 5.2. We can find that all the ODs at 600 nm are high except the Ag NWs one. It reveals that the Ag NWs has superior antibacterial property than the others.

To sum up, we provide a surfactant assisted electrochemical method to grow Ag NWs on hard substrates effectively. Applications of SERS and H_2O_2 sensing have been developed. Reduction of aromatic nitro compounds and antibacterial properties have also been investigated. We expect the Ag NWs are not only used in molecule sensing but also in industry and environmental purification.

5.2 References

1. Pradhan, N.; Pal, A.; Pal, T. *Langmuir* **2001,** *17*, 1800.
2. Ip, M.; Lui, S. L.; Poon, V. K. M.; Lung, I.; Burd, A. *J. Med. Microbiol.* **2006,** *55*, 59.
3. Lee, H. Y.; Park, H. K.; Lee, Y. M.; Kim, K.; Park, S. B. *Chem. Commun.* **2007**, 2959.
4. Oyanedel-Craver, V. A.; Smith, J. A. *Environ. Sci. Technol.* **2007,** *42*, 927.

Appendix

Table. Summary of growth conditions of different Ag samples in 50 mL rection solution at 303 K.

Sample	[$AgNO_3$]	[CTAC]	[HNO_3]	Reaction time
A	7.5 mM	X	X	15 min
B	7.5 mM	X	5 mM	30 min
C	7.5 mM	3.6 mM	X	3 hr
D	7.5 mM	3.6 mM	5 mM	2 hr
E	7.5 mM	5.4 mM	5 mM	6 hr

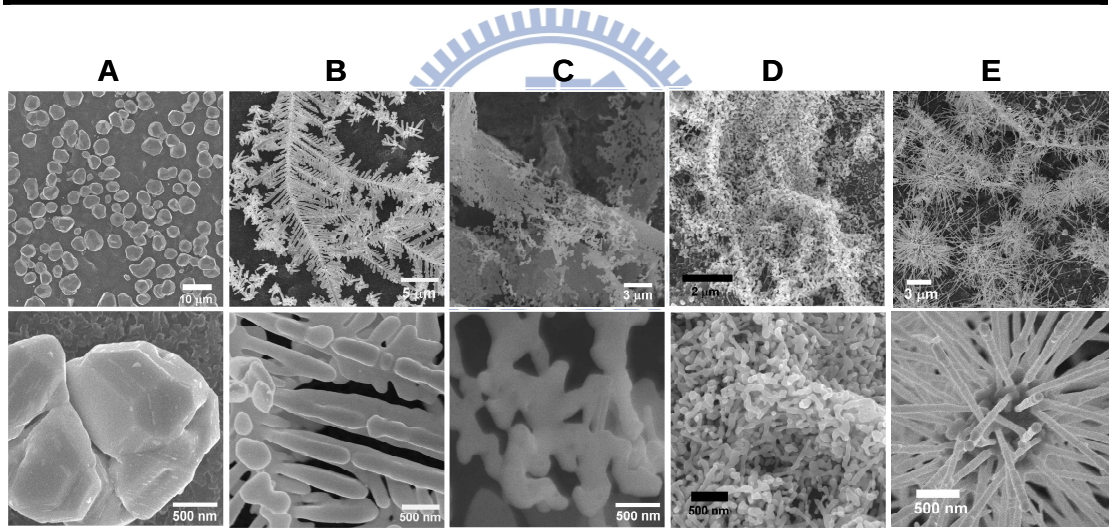

Figure. SEM images of Ag samples with different growth conditions in Table.

When the reaction solution contained $AgNO_{3(aq)}$ only, we may found Ag microparticles reduced by Cu foil on the SPC electrodes (Figure A). These structures may transform into nanodendrite and nanocoral if we added 5 mM $HNO_{3(aq)}$ and 3.6 mM $CTAC_{(aq)}$ in the solution, respectively (Figure B and C). Both $HNO_{3(aq)}$ and $CTAC_{(aq)}$ displayed the ability about anisotropic growth. For instance, the less stable facets of Ag nanostructures may oxidize $Ag_{(s)}$ into $Ag^{+}_{(aq)}$ ions by $NO_3^{-}{}_{(aq)}$ ions easily

and CTAC has been proposed as a surface capping reagent. Therefore, we combined these reagents in the reaction solution. We discovered some nanoparticles aggregated and short rodlike nanostructures on SPC electrodes (Figure D) while the $AgNO_{3(aq)}$ reaction solution consisted of 3.6 mM $CTAC_{(aq)}$ and 5 mM $HNO_{3(aq)}$. Finally, we slightly increased the CTAC concentration in sample D. We obtained lots of urchin-like Ag nanowires on SPC electrodes (Figure E).